Elevated pyramidal cell firing orchestrates arteriolar vasoconstriction through COX-2-derived prostaglandin E2 signaling

Benjamin Le Gac[1], Marine Tournissac[2], Esther Belzic [1], Sandrine Picaud[1], Isabelle Dusart[1], Hédi Soula[3], Dongdong Li[1], Serge Charpak[2], Bruno Cauli[1*]

1. Sorbonne Université, CNRS, INSERM, Neurosciences Paris Seine - Institut de Biologie Paris Seine (NPS-IBPS), 9 quai Saint Bernard, 75005 Paris, France.

2. Sorbonne Université, INSERM, CNRS, Institut de la Vision, 17 rue Moreau, 75012 Paris, France.

3. Sorbonne Université, INSERM, Nutrition and Obesities: Systemic Approaches, NutriOmics, research unit, 91 boulevard de l'hôpital, 75013 Paris, France.

*Correspondence: bruno.cauli@upmc.fr

Keywords: Neurovascular coupling, pyramidal cells, prostaglandin E2 signaling, optogenetics

Abstract

Neurovascular coupling, linking neuronal activity to cerebral blood flow, is essential for brain function and underpins functional brain imaging. Whereas mechanisms involved in vasodilation are well-documented, those controlling vasoconstriction remain overlooked. This study unravels the mechanisms by which pyramidal cells elicit arteriole vasoconstriction. Using patch-clamp recording, vascular and Ca^{2+} imaging in mouse cortical slices, we show that strong optogenetic activation of layer II/III pyramidal cells induces vasoconstriction, correlating with firing frequency and somatic Ca^{2+} increase. *Ex vivo* and *in vivo* pharmacological investigations indicate that this vasoconstriction predominantly recruits prostaglandin E2 through the cyclooxygenase-2 pathway, and activation of EP1 and EP3 receptors. We also present evidence that specific interneurons releasing neuropeptide Y, and astrocytes, through 20-hydroxyeicosatetraenoic acid, contribute to this process. By revealing the mechanisms by which pyramidal cells lead to vasoconstriction, our findings shed light on the complex regulation of neurovascular coupling.

Significance statement

Cerebral blood flow is tightly controlled by neuronal activity, a process termed neurovascular coupling which serves as the physiological basis for functional brain imaging widely used to map neuronal activity in health and diseases. While the prevailing view links increased neuronal activity with enhanced blood perfusion, our data suggest that elevated neuronal activity can also reduce cerebral blood flow. By optically controlling the activity of pyramidal cells, we demonstrate that these excitatory neurons induce vasoconstriction when their action potential firing is increased by releasing glutamate and lipid messengers. These findings update the interpretation of functional brain imaging signals and help to better understand the etiopathogenesis of epilepsy and Alzheimer's disease, in which hyperactivity, hypoperfusion and cognitive deficits overlap.

Introduction

The brain critically depends on the uninterrupted blood supply provided by a dense vasculature (Schmid et al., 2019). Cerebral blood flow (CBF) is locally and temporally controlled by neuronal activity, by an essential process called neurovascular coupling (NVC), and is impaired in early stages of numerous neurological disorders (Iadecola, 2017). NVC also serves as the physiological basis for functional brain imaging widely used to map neuronal activity. Neuronal activity increases CBF within seconds (Iadecola, 2017). In the cerebral cortex, the hyperemic response linked to neural activity is supported by dynamically controlled vasodilation that is spatially and temporally constrained by vasoconstriction in a second phase (Devor et al., 2007). Conversely, vasoconstriction and decreased CBF usually correlate with reduced neuronal activity (Devor et al., 2007; Shmuel et al., 2002).

Mounting evidence indicates that the positive correlation between neuronal activity and CBF is not always maintained under physiological conditions: i) robust sensory-evoked vasodilation can occur in the absence of substantial neuronal response (O'Herron et al., 2016), ii) conversely, pronounced neuronal activity is not systematically associated with increased hemodynamics (Ma et al., 2016), iii) CBF is decreased in several cortical areas despite local increase in neuronal activity (Devor et al., 2008), and iv) optogenetic simulation of inhibitory GABAergic interneurons results in vasodilation (Uhlirova et al., 2016). Furthermore, in pathological conditions with intense neuronal activity such as epileptic seizures, a sustained hypoperfusion induced by vasoconstriction is observed (Farrell et al., 2016; Tran et al., 2020).

NVC is achieved by the synthesis and release of vasoactive messengers within the neurovascular unit (Iadecola, 2017), which act on the contractility of mural cells (smooth muscle cells and pericytes) to control vessel caliber and CBF along the vascular tree (Rungta et al., 2018). Pial and penetrating arterioles, which have a higher density of contractile mural cells and control their diameter faster than capillaries (Hartmann et al., 2021; Hill et al., 2015; Rungta et al., 2021, 2018), play a key role in regulating CBF. Messengers of vasodilation released by excitatory neurons, GABAergic interneurons, astrocytes, or endothelial cells, include nitric oxide, K^+, arachidonic acid derivatives such as prostaglandin E2 (PGE2) (Iadecola, 2017), or more recently glutamate (Zhang et al., 2024). Despite its physio pathological importance, vasoconstriction is less understood with fewer cell types and vasoactive messengers that have been identified. It is now generally accepted that GABAergic

interneurons are key players in vasoconstriction by releasing neuropeptide Y (NPY)(Cauli et al., 2004; Uhlirova et al., 2016). Under certain conditions, astrocytes can also induce vasoconstriction via 20-hydroxyeicosatetraenoic acid (20-HETE)(Mulligan and MacVicar, 2004) or high K^+ concentration (Girouard et al., 2010). However, the involvement of pyramidal cells in vasoconstriction has been overlooked.

PGE2 has emerged as a bimodal messenger of NVC, similar to K^+ (Girouard et al., 2010) and glutamate(Zhang et al., 2024), that can induce either vasodilation (Gordon et al., 2008; Lacroix et al., 2015; Lecrux et al., 2011; Mishra et al., 2016) or vasoconstriction (Dabertrand et al., 2013; Rosehart et al., 2021) depending on its concentration and/or site of action along the vascular tree. Under physiological conditions, PGE2 is produced during NVC by either astrocytes (Mishra et al., 2016) or pyramidal cells(Lacroix et al., 2015) via the rate-limiting synthesizing enzymes cyclooxygenase-1 (COX-1) or -2 (COX-2), respectively. Since COX-2-expressing pyramidal cells can release glutamate and PGE2, both of which induce vasoconstriction at high concentrations (Dabertrand et al., 2013; Rosehart et al., 2021; Zhang et al., 2024), pyramidal cells may be responsible for vasoconstriction when their spiking activity is high.

To test this hypothesis, we used *ex vivo* and *in vivo* approaches in combination with optogenetics to precisely control pyramidal cell firing in the mouse barrel cortex while monitoring the resulting arteriolar response. We found that pyramidal cells induce vasoconstriction at high stimulation frequency and about half of them express all the transcripts required for a cell autonomous synthesis of the vasoconstrictor messengers PGE2 and prostaglandin F2α (PGF2α). Pharmacological investigations revealed that this neurogenic vasoconstriction depends on COX-2-derived PGE2 via the direct activation of vascular EP1 and EP3 receptors. It also involves the recruitment of intermediary NPY interneurons acting on the Y1 receptor, and, to a lesser extent astrocytes, via 20-HETE and COX-1-derived PGE2. Thus, our study reveals the mechanisms by which high frequency pyramidal cell firing leads to vasoconstriction.

Results

Pyramidal cells induce vasoconstriction at high firing frequency.

To determine if pyramidal cells action potential (AP) firing can induce vasoconstriction in a frequency-dependent manner, we used optogenetics to induce AP firing while monitoring the resulting vascular response in cortical slices. We used Emx1-cre;Ai32 transgenic mice expressing the H134R variant of channelrhodopsin-2 (ChR2) in the cortical glutamatergic neurons (Gorski et al., 2002), conferring robust pyramidal cell photoexcitability (Madisen et al., 2012). Wide-field photostimulation of cortical slices was achieved in layers I to III (Supplementary Fig. 1a) using 10-second trains of 5 ms light pulses (see Methods) delivered at five different frequencies (1, 2, 5, 10 and 20 Hz, Fig. 1a).

First, we ensured the efficiency of the photostimulation paradigm by recording layer II-III pyramidal cells in whole-cell current clamp mode (Fig. 1a). We observed that optogenetic stimulation resulted in the firing of an initial AP that was followed by a train of spikes whose amplitude and frequency transiently decreased before reaching a steady state (Fig. 1a, upper traces). Consistent with the kinetic properties of the H134R ChR2 variant (Lin et al., 2009) and the intrinsic firing properties of pyramidal cells (Karagiannis et al., 2009), the steady-state firing frequency matched the photostimulation frequency up to 5 Hz but was lower at higher frequencies (Fig. 1a, steady-state spike success rate: 100 ± 0 % at 1, 2 and 5 Hz, 70 ± 11 % at 10 Hz and 55 ± 12 % at 20 Hz). These observations demonstrate efficient pyramidal cell activation over a wide range of photostimulation frequencies.

To test the hypothesis that neuronal activity induces vasoconstriction, we analyzed the optogenetically induced response of penetrating arterioles. Layer I arterioles were imaged for 30 minutes in cortical slices (Supplementary Fig.2; Supp. table 1) without preconstriction to facilitate observation of vasoconstriction (Cauli et al., 2004). Examination of the evoked vascular response over 30-minutes (Supplementary Fig.2) showed that increasing the frequency of photostimulation shifted the overall vascular response from a barely discernible delayed response between 1 Hz and 5 Hz to a sustained vasoconstriction at 10 Hz and above which began less than 2 minutes after photostimulation (10 Hz: 1.4 ± 0.4 min; 20 Hz: 1.6 ± 0.5 min). Most vessels (n= 8 of 10 arterioles) showed a strong and rapid vasoconstriction at 20 Hz. On average, this response peaked at 6.8 ± 2.4 min, much earlier than at lower frequencies,

115 which typically required more than 10 min to reach a maximum (Supplementary Fig.2c, 1 Hz:
116 15.6 ± 4.0 min; 2 Hz: 13.2 ± 2.3 min; 5 Hz: 16.0 ± 3.6 min; 10 Hz: 15.7 ± 2.4 min). Because the
117 vascular response shifted to reliable vasoconstriction, with onset and peak in less than 2 and
118 10 minutes, respectively, similar to previous observations in cortical slices (Cauli et al., 2004),
119 when the frequency of photostimulation was increased to 20 Hz, we defined the first 10
120 minutes of recording as the vasoconstriction time frame for subsequent comparisons and
121 analyses. While photostimulation at 1 to 5 Hz failed to elicit fast reliable vascular responses
122 (Fig. 1c-d), 10 Hz photostimulation predominantly induced vasoconstriction (n= 4 of 5
123 arterioles, Fig. 1 c-d, area under the curve (AUC)= -1.7 ± 1.1 x 10^3 %.s, n= 5). This response was
124 even more pronounced at 20 Hz, as all arterioles showed vasoconstriction of high magnitude
125 (Fig. 1 b-d; AUC= -3.7 ± 0.7 x 10^3 %.s, $F_{(4, 30)}$= 6.135, p= 9.89 x 10^{-4}, one-way ANOVA, n= 10
126 arterioles). This difference was particularly striking when comparing the magnitude at 20 Hz
127 (Fig. 1d) with those at 1 Hz ($t_{(12)}$= -3.48, p= 0.0407, t-test), 2 Hz ($t_{(18)}$= -4.09, p= 0.0250, t-test)
128 and 5 Hz ($t_{(14)}$= -3.7, p= 0.0346, t-test). Intense optogenetic stimulation of pyramidal cells has
129 been shown to elicit cortical spreading depression (Chung et al., 2018), which induces
130 vasoconstriction (Zhang et al., 2024) and fast cell swelling (Zhou et al., 2010). We ruled out
131 this possibility by showing that the rate of change in light transmittance associated with cell
132 swelling remained below that of cortical spreading depression (Zhou et al., 2010)
133 (Supplementary Table 1). On the other hand, ChR2-independent vascular changes induced by
134 high light intensity have been reported (Rungta et al., 2017). We verified that 20 Hz
135 photostimulation did not induce a vascular response in wild-type mice that do not express
136 ChR2 (Supplementary Fig.1). Taken together, our observations indicate that photostimulation
137 of pyramidal cells produces a frequency-dependent vasoconstriction.

138 **Optogenetic stimulation induces a frequency-dependent, gradual increase in somatic**
139 **calcium that precedes the vascular response.**

140 These observations raise the questions of how pyramidal neurons can induce vasoconstriction
141 at higher AP-firing rates. It is generally accepted that the synthesis and/or release of
142 vasodilatory substances requires an increase in intracellular Ca^{2+} in the releasing cells (Attwell
143 et al., 2010; Cauli and Hamel, 2010), but little is known about the release of vasoconstricting
144 substances. We therefore determined whether an increase in somatic Ca^{2+} concentration in
145 cortical neurons was also dependent on photostimulation frequency. We combined

146 optogenetic stimulation with whole-cell current clamp recording and intracellular Ca^{2+}
147 imaging using Rhod-2 delivered by patch pipette (Fig. 2a). Excitation of this red Ca^{2+} indicator
148 at 585 nm did not induce any voltage response in the recorded pyramidal cells (Fig. 2a), as
149 expected from the action spectrum of ChR2 (Lin et al., 2009). In contrast, photostimulation at
150 470 nm elicited a train of spikes accompanied by a somatic Ca^{2+} increase that decayed for tens
151 of seconds after photostimulation without triggering any significant recurrent spiking activity
152 (Supplementary Fig. 3). The Ca^{2+} response evoked by 20 Hz photostimulation was more than
153 twice of that evoked by 2 Hz photostimulation (Fig. 2b; 2 Hz: $\Delta F/F_0$= 34.5 ± 3.7 %, n= 9 cells,
154 vs. 20 Hz: $\Delta F/F_0$= 79.5 ± 17.7 %, n= 9 cells; $t_{(16)}$= 2.485, p= 0.024397), while the average number
155 of evoked spikes was about five times higher (Fig. 1a and supplementary Fig. 3). These results
156 demonstrate a frequency-dependent increase in intracellular Ca^{2+} induced by
157 photostimulation, that precedes vasoconstriction. We therefore aimed to understand the
158 molecular mechanisms linking neuronal activity to vasoconstriction.

159 **Vasoconstriction induced by pyramidal cells requires AP firing and is partially dependent on**
160 **glutamatergic transmission.**

161 In pyramidal cells, APs induce both somatic Ca^{2+} elevation (Smetters et al., 1999) and
162 glutamate release. To determine whether spiking activity is required for vasoconstriction
163 induced by 20 Hz photostimulation, we blocked APs with the voltage-activated sodium
164 channel blocker tetrodotoxin (TTX, 1 µM, n= 6 arterioles). This treatment completely
165 abolished the vasoconstriction evoked by 20 Hz photostimulation (Fig. 3; AUC= 0.4 ± 0.4 x
166 10^3 %.s, $t_{(14)}$= 5.57, p= 8.6656 x 10^{-6}). These data indicate that APs are mandatory for
167 neurogenic vascular response and may involve glutamate release.

168 Indeed, high levels of glutamate released from pyramidal cells may activate NPY-expressing
169 interneurons or astrocytes through activation of ionotropic or group I metabotropic glutamate
170 receptors (Girouard et al., 2010; Mulligan and MacVicar, 2004; Uhlirova et al., 2016). It may
171 also directly activate NMDA receptors on arteriolar smooth muscle cells, resulting in a large
172 intracellular Ca^{2+} increase and subsequent vasoconstriction (Zhang et al., 2024). To test the
173 hypothesis that glutamate from pyramidal cells, either directly or indirectly, results in
174 vasoconstriction, we blocked glutamatergic transmission by antagonizing AMPA/kainate,
175 NMDA and group I metabotropic receptors expressed by cortical neurons (Tasic et al., 2016;
176 Zeisel et al., 2015) and juvenile astrocytes(Sun et al., 2013). Glutamate receptor antagonists

177 reduced the magnitude of vasoconstriction (-1.6 ± 0.4 x 10^3 %.s, $t_{(18)}$= 3.28, p= 0.0160) by
178 approximately half (Fig. 3). Taken together, our data suggest that photostimulation of
179 pyramidal cells elicits a frequency-dependent vasoconstriction that requires AP firing and
180 partially involves glutamatergic transmission. We therefore sought to elucidate the
181 glutamate-independent vasoactive pathway underlying this neurogenic vascular response.

182 **Pyramidal cells express the mRNAs for a cell autonomous PGE2 and PGF2α synthesis**

183 Several arachidonic acid metabolites produced after intracellular Ca^{2+} elevation, including
184 PGF2α, but also PGE2, exert dose-dependent vasoconstrictive effects (Dabertrand et al., 2013;
185 Rosehart et al., 2021; Zonta et al., 2003). These prostaglandins could therefore be
186 progressively released as the frequency of photostimulation and somatic Ca^{2+} increase, and
187 thereby promote vasoconstriction. Layer II-III pyramidal cells have been shown to produce
188 PGE2 (Lacroix et al., 2015). To determine whether the synthesizing enzymes of PGE2 and
189 PGF2α are present in pyramidal cells, we performed single-cell RT-PCR after patch-clamp
190 recording (Devienne et al., 2018). Sixteen layer II-III pyramidal cells were visually identified
191 based on the triangular shape of their soma and a prominent apical dendrite. Their
192 glutamatergic phenotype was confirmed both by their stereotypical regular spiking firing
193 pattern (Fig. 4a) and also by the expression of the vesicular glutamate transporter, vGlut1, and
194 neither of the two GABA synthesizing enzymes, thus excluding possible contamination by
195 GABAergic interneurons (Fig. 4b)(Karagiannis et al., 2009). The rate-limiting enzymes of
196 prostaglandin synthesis, cyclooxygenase-1 (COX-1) and -2 (COX-2), were detected in 25% (n=
197 4 of 16 cells) and 31% (n= 5 of 16 cells) of pyramidal cells, respectively, (Fig. 4b-d) but were
198 never co-expressed (Fig. 4d). The cytosolic enzyme responsible for synthesizing PGE2 (cPGES)
199 was observed in most pyramidal cells (Fig. 4b-c; 88%, n= 14 of 16 cells). In addition, the
200 microsomal PGES, mPGES1 and mPGES2 were detected in 6% (Fig. 4c, n= 1 of 16 cells) and
201 38% (Fig. 4b,c; n= 6 of 16 cells) of pyramidal cells, respectively, and were always co-expressed
202 with cPGES. The PGF2α terminal-synthesizing enzyme AKR1B3 was observed in the majority
203 of neurons (Fig. 4b-c; n= 11 of 16 cells, 69%). Occasionally, it was co-detected with the
204 prostamide/prostaglandin F synthase (PM-PGFS, Fig. 4c, n= 5 of 16 cells, 31%) and the PGE2
205 converting enzyme carbonyl reductase 1 (CBR1, Fig. 4c; n= 3 of 16 cells, 19%). CBR1 was
206 consistently detected alongside at least one PGES. Pyramidal cells positive for COX-1 also
207 expressed PGES (Fig. 4d), with most of them also co-expressing PGFS (n=3 out of 4). All

208 neurons positive for COX-2 co-expressed both PGES and PGFS (Fig. 4d). These molecular
209 observations suggest that subpopulations accounting for about half of layer II-III pyramidal
210 cells express all the transcripts necessary for the synthesis of PGE2 and PGF2α .

211 **Prostaglandins underpin vasoconstriction *ex vivo* and *in vivo*.**

212 To investigate whether prostaglandins could mediate neurogenic vasoconstriction, we
213 inhibited their synthesis. In cortical slices, the non-selective COX inhibitor indomethacin (5
214 µM, supplementary Table 3, Fig. 5a and b) completely abolished the vascular response (n= 10
215 arterioles, AUC= 0.0 ± 0.2 x 10^3 %.s, $t_{(18)}$= 5.86, p= 3.4385 x 10^{-5}). To verify that high-frequency
216 stimulation of pyramidal cells also induces vasoconstriction *in vivo*, 10 Hz photostimulation
217 was reproduced in anesthetized Emx1-cre;Ai32 mice. Pial arterioles diameter measured by 2-
218 photon line scan imaging (Fig. 5c and d) revealed that pyramidal cells induce vasodilation (1st
219 phase) followed by sustained vasoconstriction (2nd phase, Fig. 5d and e). The constriction
220 phase was inhibited by indomethacin (i.v.), indicating the involvement of prostaglandins in the
221 vasoconstriction (AUC_{Ctrl}= -291.5 ± 92.4 %.s vs. $AUC_{Indo.}$= 332.4 ± 184.4 %.s, $U_{(5,4)}$= 0, p= 0.0159,
222 Fig. 5d-f), which confirms our *ex vivo* observations. To determine whether they originated
223 from COX-1 or COX-2 activity, we utilized selective inhibitors in cortical slices. The
224 vasoconstriction magnitude was reduced by the COX-1 inhibitor SC-560 (100 nM, n= 10
225 arterioles, supplementary Table 3) (-1.4 ± 0.7 x 10^3 %.s, $t_{(18)}$= 3.54, p= 9.3396 x 10^{-3}, Fig. 5a-b).
226 The COX-2 inhibitor NS-398 (10 µM, n= 7 arterioles, supplementary Table 3) completely
227 abolished pyramidal cell-induced vasoconstriction in a more potent manner (Fig. 5a-b; AUC=
228 0.1 ± 0.3 x 10^3 %.s, $t_{(15)}$= 5.45, p= 1.0853 x 10^{-5}), mimicking the *ex vivo* effect of indomethacin.
229 These observations suggest that prostaglandins, derived mainly from COX-2 activity, and to a
230 lesser extent from COX-1 activity, mediate pyramidal cell-induced vasoconstriction.

231 **PGE2 mediates vasoconstriction by acting primarily on EP1 receptor.**

232 To determine the nature of the prostaglandins and their receptors, we selectively antagonized
233 the vasoconstrictor receptors of PGE2, EP1 or EP3, or the FP receptor of PGF2α. The
234 magnitude of vasoconstriction was reduced by the selective EP1 receptor antagonist ONO-
235 8130 (10 nM, n= 9 arterioles, Fig. 5g-h, 0.3 ± 0.3 x 10^3 %.s, $t_{(17)}$= 6.01, p= 2.8451 x 10^{-6},
236 supplementary Table 3), and to a lesser extent, by the EP3 receptor antagonist L-798,106 (1
237 µM, n= 9 arterioles, Fig. 5 g-h, -0.9 ± 0.4 x 10^3 %.s, $t_{(17)}$= 4.30, p= 8.0261 x 10^{-4}, supplementary
238 Table 3). Impairing FP receptor signaling with AL-8810 (10 µM, n= 9 arterioles, Fig. 5 g-h,

239 Supplementary table 3) tended to reduce the evoked vasoconstriction, however, it did not
240 reach statistical significance (AUC= -1.9 ± 0.4 x 10^3 %.s, $t_{(17)}$= 2.82, p= 0.0533). Additionally, the
241 pre-constricted state induced by this weak partial FP agonist (Sharif and Klimko, 2019)
242 (supplementary Fig. 6f) resulted in a diameter reduction of approximately 4% (diameter
243 before application 21.8 ± 2.5 µm vs. during 20.9 ± 2.6 µm, n= 9 arterioles, $t_{(8)}$= 2.374, p=
244 0.0457, paired t-test), which underestimated the optogenetic vascular response. Taken
245 together, these results indicate that pyramidal cell photoactivation induces vasoconstriction
246 through the release of PGE2 originating mainly from COX-2. This effect primarily acts on the
247 EP1 receptor and, to a lesser extent, on the EP3 receptor.

248 To test a direct effect of PGE2 through vascular EP1/EP3 activation, we determined whether
249 exogenous agonists of PGE2 receptors could mimic the vasoconstriction induced by pyramidal
250 cell photostimulation. Similar to increasing photostimulation frequencies, exogenous
251 application of PGE2 induced vasoconstriction in a dose-dependent manner which persisted
252 for several minutes after removal (Supplementary Fig. 7a). Likewise, 10 µM sulprostone, an
253 EP1/EP3 agonist with an EC_{50} comparable to that of PGE2 (Boie et al., 1997), mimicked the
254 vasoconstriction induced by 1-10 µM PGE2 (Supplementary Fig. 7b). Application of 10 µM
255 PGE2 in the presence of TTX did not impair the evoked vasoconstriction (Supplementary Fig.
256 7c). These observations suggest that PGE2 and its EP1 and EP3 receptors mediate a sustained
257 neurogenic vasoconstriction and that once PGE2 is released, its constrictive effect is
258 independent of AP firing.

259 **Astrocytes through 20-HETE and NPY interneurons are indirect intermediates of pyramidal**
260 **cell-induced vasoconstriction.**

261 In addition to smooth muscle cells, PGE2 released by pyramidal cells can also activate
262 astrocytes and neurons (Clasadonte et al., 2011; Di Cesare et al., 2006), which also express its
263 receptors (Tasic et al., 2016; Zeisel et al., 2015). To assess whether astrocytes could mediate
264 the PGE2-dependent vasoconstriction, we first targeted the large conductance Ca^{2+}-activated
265 (BK) channels and the 20-HETE pathways, both of which mediate astrocyte-derived
266 vasoconstriction dependent on glutamatergic transmission (Girouard et al., 2010; Mulligan
267 and MacVicar, 2004). Blockade of BK channels with paxilline (1 µM, n= 10 arterioles,
268 Supplementary table 3) did not impair the vascular response (Fig. 6; AUC = -3.7 ± 0.3 x 10^3 %.s,
269 $t_{(18)}$ = 0.03, p = 1). Selective inhibition of the 20-HETE synthesizing enzyme, CYP450 ω-

270 hydroxylase, with HET-0016 (100 nM, n= 10 arterioles, Supplementary table 3) reduced the
271 magnitude of the evoked vasoconstriction (Fig. 6; AUC = -1.6 ± 0.7 x 10^3 %.s, $t_{(18)}$ = 3.32, p =
272 0.0160). These data suggest that astrocytes partially mediate the vasoconstriction induced by
273 pyramidal cells via 20-HETE but not via K^+ release. We next determined whether NPY, a potent
274 vasoconstrictor (Cauli et al., 2004), was involved in neurogenic vasoconstriction. Antagonism
275 of the NPY Y1 receptors by BIBP3226 (1 µM, n= 10 arterioles, Supplementary table 3) abolished
276 neurogenic vasoconstriction (Fig. 6; AUC = -0.3 ± 0.2 x 10^3 %.s, $t_{(18)}$ = 5.28, p = 1.9512 x 10^{-5}).
277 These results suggest that neurogenic vasoconstriction induced by pyramidal cell
278 photostimulation involves NPY release and the activation of Y1 receptors (Cauli et al., 2004;
279 Karagiannis et al., 2009; Uhlirova et al., 2016) and astrocytes via 20-HETE in a glutamatergic-
280 dependent and -independent manner.

281 **Discussion**

282 This study establishes that pyramidal cell activity leads to arteriolar vasoconstriction, and that
283 the magnitude of the vasoconstriction depends on AP firing frequency and correlates with a
284 graded increase in pyramidal cell somatic Ca^{2+}. This vascular response partially involves
285 glutamatergic transmission through direct and indirect mechanisms on arteriolar smooth
286 muscle cells. *Ex vivo* and *in vivo* observations revealed that PGE2, predominantly produced by
287 layer II-III COX-2 pyramidal cells, and its EP1 and EP3 receptors play a crucial role in neurogenic
288 vasoconstriction. Pharmacological evidence indicates that some interneurons, via NPY release
289 and activation of Y1 receptors, and to a lesser extent, astrocytes through 20-HETE and possibly
290 COX-1 derived PGE2 play an intermediary role in this process (Figure 7).

291 We found that increasing the frequency of photostimulation in an *ex vivo* preparation caused
292 nearby arteriole to go from a barely discernible response to robust vasoconstriction. In
293 contrast, *in vivo* observations have shown that the optogenetic stimulation of pyramidal cells
294 results in a biphasic response: a fast hyperemic/vasodilatory response (Kahn et al., 2013;
295 Lacroix et al., 2015; Scott and Murphy, 2012), that is followed by a pronounced
296 vasoconstriction (Uhlirova et al., 2016)(Fig. 5). The slow kinetics of the vascular response
297 observed *ex vivo* is comparable with previous observations in slices (Cauli et al., 2004; Rancillac
298 et al., 2006), and is likely due to the lower recording temperature compared to *in vivo*, which
299 slows the synthesis of vasoactive mediators (Rancillac et al., 2006) and downstream reactions.
300 The difficulty in observing vasodilation in cortical slices may be due to relaxed arterioles which
301 favor vasoconstriction(Blanco et al., 2008). The evidence that neurogenic vasoconstriction is
302 frequency-dependent (Fig. 1) and that pharmacologically-induced vasoconstriction persists in
303 preconstructed (Girouard et al., 2010) or pressurized arterioles (Dabertrand et al., 2013),
304 suggests that the neurogenic vasoconstriction primarily depends on a high pyramidal cell firing
305 rate rather than on vascular tone.

306 Most previous observations did not report a decreased in CBF induced by optogenetic
307 stimulation of pyramidal cells *in vivo* (Lacroix et al., 2015; Scott and Murphy, 2012). This may
308 be attributed to differences in the photostimulation paradigm and/or the specific subtype of
309 pyramidal cells that were stimulated. In our study, we used 10 seconds of photostimulation
310 both *in vivo* and *ex vivo*. Earlier studies have employed shorter photostimulation times, lasting
311 no more than 1 second (Lacroix et al., 2015; Scott and Murphy, 2012; Uhlirova et al., 2016),

312 which may have resulted in an insufficient number of elicited APs to induce robust
313 vasoconstriction. Furthermore, we observed that neurogenic vasoconstriction is highly
314 dependent on COX-2, which is primarily expressed in layer II-III pyramidal cells (Lacroix et al.,
315 2015; Tasic et al., 2016; Zeisel et al., 2015). In our study, photostimulation of almost all
316 pyramidal cells in Emx1-Cre;Ai32 mice (Gorski et al., 2002; Madisen et al., 2012) likely resulted
317 in the release of more COX-2 metabolites. Thy1-ChR2 mice used in previous studies (Scott and
318 Murphy, 2012; Uhlirova et al., 2016), on the other hand, express primarily ChR2 in layer V
319 pyramidal cells (Kahn et al., 2013), which more rarely express COX-2.

320 Our *ex vivo* and *in vivo* observations revealed that PGE2, primarily derived from COX-2, plays
321 a critical role in neurogenic vasoconstriction by activating EP1 and EP3 receptors expressed by
322 vascular smooth muscle cells (Zhang et al., 2024). Previous studies have shown that COX-2
323 pyramidal cells, when activated *in vivo* by sensory stimulation or *ex vivo*, induce a NMDA-
324 dependent increase in CBF and vasodilation through PGE2 and EP2/EP4 receptors (Lacroix et
325 al., 2015; Lecrux et al., 2011; Niwa et al., 2000). Differences in the levels and/or sites of action
326 of released PGE2 may explain the absence of secondary vasoconstriction. In Emx1-Cre;Ai32
327 mice (Gorski et al., 2002; Madisen et al., 2012), optogenetic stimulation may have activated a
328 greater number of COX-2 pyramidal cells and resulted in a higher local release of PGE2
329 compared to sensory stimulation. Furthermore, since PGE2 is barely catabolized in the
330 cerebral cortex (Alix et al., 2008), most of its removal occurs across the blood-brain barrier by
331 specific transporters. The lack of blood perfusion in brain slices may impaired this clearance
332 mechanism, leading to PGE2 accumulation. It is noteworthy that the PGE2-induced
333 vasoconstriction persisted after its removal (supplementary figure 7). A high level of PGE2 may
334 have facilitated the activation of the EP1 receptor, which has a lower affinity than the EP2/EP4
335 receptors (Boie et al., 1997). Additionally, it may have promoted the rapid desensitization of
336 the dilatory EP4 receptor (Desai et al., 2000) thereby favoring vasoconstriction. Furthermore,
337 PGE2 can induce either EP1-dependent arteriolar dilation or constriction depending on
338 whether it is locally applied to capillaries or arterioles. Constriction prevails when both
339 segments are exposed (Rosehart et al., 2021). Our photostimulation focused on superficial
340 penetrating arterioles, which lack a capillary network in their close vicinity (Kasischke et al.,
341 2011). This may have facilitated the direct EP1-mediated arteriolar constriction (Dabertrand
342 et al., 2013; Rosehart et al., 2021). Overall, these observations suggest that COX-2 pyramidal

343 cells can sequentially promote both vasodilation and vasoconstriction through the release of
344 PGE2, depending on the context.

345 Consistent with previous reports in rodents (Lacroix et al., 2015; Tasic et al., 2016; Yamagata
346 et al., 1993; Zeisel et al., 2015), the transcripts of the rate-limiting enzymes COX-1 and COX-2,
347 were detected in subpopulations of mouse layer II-III pyramidal cells, respectively. COX-1/2
348 expression was found to be systematically associated with at least one PGE2 synthesizing
349 enzyme. The major isoforms were cPGES and mPGES2, with the latter being less prevalent
350 (Lacroix et al., 2015; Tasic et al., 2016; Zeisel et al., 2015). The low detection rate of mPGES1,
351 an isoform co-induced with COX-2 by various stimuli (Takemiya et al., 2007; Yamagata et al.,
352 2001), reflects its low constitutive basal expression level. The presence of PM-PGFS, CBR1 and
353 AKR1B3 in layer II-III pyramidal cells is consistent with single-cell RNAseq data (Tasic et al.,
354 2016; Zeisel et al., 2015). The expression of a PGFS was systematically observed in COX-2
355 positive pyramidal cells and in a majority of COX-1 positive neurons, similar to PGES. These
356 observations collectively indicate that subpopulations of layer II-III pyramidal cells express the
357 mRNAs required for PGE2 and PGF2α synthesis derived from COX-1 or COX-2 activity. Our
358 pharmacological observations did not reveal a contribution of PGF2α in neurogenic
359 vasoconstriction, despite the potential ability of pyramidal cells to produce it. This is likely
360 because PGF2α is only detectable in pyramidal neurons under conditions where COX-2 is over-
361 expressed (Takei et al., 2012).

362 Pyramidal cells may have an indirect effect on vascular activity through the activation of
363 intermediate cell types, in addition to the direct vascular effects of PGE2 and glutamate (Zhang
364 et al., 2024). Consistent with previous observations, we found that glutamate transmission
365 from pyramidal cells is involved to some extent (Uhlirova et al., 2016). Additionally, we found
366 that the NPY Y1 receptor plays a key role in neurogenic vasoconstriction. It is likely that
367 glutamatergic transmission contributed to NPY release, considering that NPY GABAergic
368 interneurons express a wide range of ionotropic and metabotropic glutamate receptors (Tasic
369 et al., 2016; Zeisel et al., 2015). Consistently, the Y1 receptor has been shown to be involved
370 in vasoconstriction induced by sensory and optogenetic stimulation of GABAergic
371 interneurons (Uhlirova et al., 2016). Activation of group I metabotropic receptors in
372 perivascular astrocytes has been shown to promote vasoconstriction via BK channel-
373 dependent K^+ release (Girouard et al., 2010) or 20-HETE (Mulligan and MacVicar, 2004).

374 However, the neurogenic vasoconstriction was not affected by the blockade of BK channels,
375 which rules out this astrocytic pathway. In contrast, the inhibition of ω-hydroxylase partially
376 reduced neurogenic vasoconstriction, suggesting the involvement of 20-HETE. Additionally,
377 astrocytes may also have contributed to vasoconstriction through the release of PGE2 derived
378 from COX-1 (Attwell et al., 2016), as indicated by its mild impairment under SC-560.

379 The observation that both EP1 and Y1 antagonists abolished the vasoconstriction suggests
380 that PGE2 and NPY may act in series, possibly with PGE2 activating NPY interneurons via the
381 EP1 receptor. However, NPY interneurons barely express its transcript (Tasic et al., 2016; Zeisel
382 et al., 2015) and PGE2 constricts arterioles independently of AP firing, suggesting a direct
383 vascular effect of PGE2. Nevertheless, PGE2 may have facilitated NPY release via pre- and
384 postsynaptic EP2-signaling which have been shown to facilitate glutamate release(Sang et al.,
385 2005) and to induce neuronal firing (Clasadonte et al., 2011), respectively. In *ex vivo* relaxed
386 arterioles, where vasoconstriction is favored (Blanco et al., 2008), G_q or G_i signaling of EP1 or
387 Y1 receptors, respectively, appears sufficient to induce vasoconstriction. *In vivo*, where blood
388 flow both induces myogenic tone and allows PGE2 clearance, NPY and PGE2 could
389 synergistically promote vasoconstriction by decreasing and increasing cAMP and Ca^{2+} levels,
390 respectively, in smooth muscle cells. PGE2 and NPY may also exert temporally distinct
391 vasoconstrictor effects. Indeed, exogenous application of NPY induces a rapid and transient
392 vasoconstriction that returns to baseline levels after removal (Cauli et al., 2004), whereas
393 PGE2-induced vasoconstriction is slower and more persistent (supplementary figure 7). The
394 more transient effect of NPY likely reflects the presence of multiple NPY-degrading
395 enzymes(Wagner et al., 2015) and/or the desensitization of the Y1 receptor (Gicquiaux et al.,
396 2003, 2002; Tsurumaki et al., 2002) which is not the case for PGE2 (Alix et al., 2008) and its
397 vasoconstrictor receptors.

398 The time-locked photostimulation of virtually all pyramidal cells would have resulted in
399 hypersynchrony, a phenomenon that can be observed during sleep/wake transitions (Asadi-
400 Pooya and Sperling, 2019) or in pathological conditions such as epileptic seizures (Jiruska et
401 al., 2013) and in early stages of Alzheimer's disease (Bezzina et al., 2015; Palop et al., 2007).
402 Although vasoconstriction observed in epilepsy (Farrell et al., 2016) exhibits similarities to the
403 neurogenic vasoconstriction described herein, there are notable differences between the two.
404 Like neurogenic vasoconstriction, seizure-induced hypoperfusion is dependent on COX-2

405 (Farrell et al., 2016; Tran et al., 2020) and, to some extent on PGE2 (Farrell et al., 2016), likely
406 through EP1 and/or EP3 receptors. However, epileptic seizures induce the overexpression of
407 both COX-2 and mPGES1 (Takemiya et al., 2007; Yamagata et al., 1993) as well as the ectopic
408 expression of NPY (Baraban, 2004). Similar transcriptional upregulations have also been
409 reported in Alzheimer's disease (Bezzina et al., 2015; Chaudhry et al., 2008; Palop et al., 2007;
410 Pasinetti and Aisen, 1998) Additionally, PGF2α synthesis by COX-2 pyramidal cells is also
411 observed during seizures (Takei et al., 2012). Taken together, these observations suggest that
412 the mechanisms governing neurogenic vasoconstriction are exacerbated in pathological
413 hypersynchrony and may represent potential therapeutic targets.

414 Here, using multidisciplinary approaches, we describe a new mechanism of vasoconstriction
415 that depends on a high firing rate of pyramidal cells. This neurogenic vasoconstriction
416 primarily involves the release of COX-2-derived PGE2 and activation of EP1 and EP3 receptors.
417 It is mediated by direct effects on vascular smooth muscle cells but also by indirect
418 mechanisms involving NPY release from GABAergic interneurons and astrocytes by 20-HETE
419 synthesis. In contrast to previously described mechanisms of neurogenic vasoconstriction,
420 that have been mostly associated with GABAergic interneurons and neuronal inhibition (Cauli
421 et al., 2004; Devor et al., 2007; Krawchuk et al., 2020; Lee et al., 2020; Uhlirova et al., 2016),
422 our data suggest the involvement of glutamatergic excitatory neurons and increased neuronal
423 activity. This finding will help to update the interpretation of the functional brain imaging
424 signals used to map network activity in health and disease(Iadecola, 2017; Zhang and Raichle,
425 2010). This excitatory form of neurogenic vasoconstriction may also help to understand the
426 etiopathogenesis of epilepsy (Farrell et al., 2016; Tran et al., 2020) and Alzheimer's disease
427 (Palop and Mucke, 2010) in which increased cortical network activity and hypoperfusion often
428 overlap.

429 **Materials and methods**

430 **Animals**

431 Homozygous Emx1-Cre mice [Jackson Laboratory, stock #005628, B6.129S2-Emx1$^{tm1(cre)Krj}$/J
432 (Gorski et al., 2002)] were crossed with homozygous Ai32 mice [Jackson Laboratory, stock
433 #012569, B6;129S-Gt(ROSA)26Sor$^{tm32(CAG-COP4*H134R/EYFP)Hze}$/J (Madisen et al., 2012)] to obtain
434 heterozygous Emx1$^{cre/WT}$;Ai32$^{ChR2/WT}$ mice for optogenetic stimulations. C57BL/6RJ mice were
435 used for PGE2 and sulprostone exogenous applications, control optogenetic experiments and

436 single-cell RT-PCR. 16-21 postnatal day-old females and males were used for all *ex vivo*
437 experiments. Female Emx1$^{cre/WT}$;Ai32$^{ChR2/WT}$ mice, 3 to 5-month-old, were used for *in vivo*
438 experiments.

439 All experimental procedures using animals were carried out in strict accordance with French
440 regulations (Code Rural R214/87 to R214/130) and conformed to the ethical guidelines of the
441 European Communities Council Directive of September 22, 2010 (2010/63/UE). Mice were fed
442 *ad libitum* and housed in a 12-hour light/dark cycle. *In vivo* experiments were done in
443 accordance with the Institut national de la santé et de la recherche médicale (Inserm) animal
444 care and approved by the ethical committee Charles Darwin (Comité national de réflexion
445 éthique sur l'expérimentation animale – n°5) (protocol number #27135 2020091012114621).

446 ***Ex vivo* slice preparation**

447 Mice were deeply anesthetized by isoflurane (IsoVet, Piramal Healthcare UK or IsoFlo,
448 Axience) evaporation in an induction box then euthanized by decapitation. The brain was
449 quickly removed and placed in cold (~4°C), oxygenated artificial cerebrospinal fluid (aCSF)
450 containing (in mM): 125 NaCl, 2.5 KCl, 1.25 NaH2PO4, 2 CaCl2, 1 MgCl2, 26 NaHCO3, 10
451 glucose, 15 sucrose and 1 kynurenic acid (Sigma-Aldrich). 300 µm-thick coronal slices
452 containing the barrel cortex were cut with a vibratome (VT1000s; Leica) and were allowed to
453 recover at room temperature for at least 45 min with oxygenated aCSF (95% O2/5%
454 CO2)(Devienne et al., 2018). The slices were then transferred to a submerged recording
455 chamber and perfused continuously at room temperature (20-25 °C) at a rate of 2 ml/min with
456 oxygenated aCSF lacking kynurenic acid.

457 **Whole-cell recordings**

458 Patch pipettes (5.5 ± 0.2 MΩ) pulled from borosilicate glass were filled with 8 µl of RNase free
459 internal solution containing (in mM): 144 K-gluconate, 3 MgCl2, 0.5 EGTA, 10 HEPES, pH 7.2
460 (285/295 mOsm). For electrophysiological recordings combined with calcium imaging, EGTA
461 was replaced by 200 µM Rhod-2 (20777, Cayman chemicals). Whole-cell recordings were
462 performed using a patch-clamp amplifier (Axopatch 200B, MDS). Data were filtered at 5-10
463 kHz and digitized at 50 kHz using an acquisition board (Digidata 1440, MDS) attached to a
464 personal computer running pCLAMP 10.2 software package (MDS). Electrophysiological
465 properties were determined in current-clamp mode (Karagiannis et al., 2009). Membrane
466 potential values were corrected for theoretical liquid junction potential (−15.6 mV). Resting

467 membrane potential of neurons was measured immediately after passing in whole-cell
468 configuration. Only neurons with a resting membrane potential more hyperpolarized than −60
469 mV were analyzed further.

470 **Optogenetic stimulation**

471 Optogenetic stimulation was achieved through the objective using a 470 nm light emitting
472 device (LED, CoolLED, Precise Excite) attached to the epifluorescence port of a BX51WI
473 microscope (Olympus) and a set of multiband filters consisting of an excitation filter (HC
474 392/474/554/635, Semrock), a dichroic mirror (BS 409/493/573/652, Semrock), and an
475 emission filter (HC 432/515/595/730, Semrock). Photostimulation consisted of a 10-s train of
476 5 ms light pulses at an intensity of 38 mW/mm² and delivered at five different frequencies (1,
477 2, 5, 10 and 20 Hz).

478 **Infrared imaging**

479 Blood vessels and cells were observed in slices under infrared illumination with Dodt gradient
480 contrast optics (IR-DGC, Luigs and Neumann) using a double-port upright microscope
481 (BX51WI, Olympus) and a collimated light emitting device (LED; 780 nm; ThorLabs) as the
482 transmitted light source, a 40X (LUMPlanF/IR, 40X/0.80 W, Olympus) or a 60X (LUMPlan FL/IR
483 60X/0.90 W, Olympus) objective and a digital camera (OrcaFlash 4.0, Hamamatsu) attached to
484 the front port of the microscope. Penetrating arterioles in layer I were selected by IR-DGC
485 videomicroscopy based on their well-defined luminal diameter (10-40 µm), their length
486 remaining in the focal plane for at least 50 µm (Lacroix et al., 2015), and the thickness of their
487 wall (4.1 ± 0.1 µm, n = 176 blood vessels). A resting period of at least 30 min (Zonta et al.,
488 2003) was observed after slice transfer. After light-induced responses, arteriolar contractility
489 was tested by the application of aCSF containing the thromboxane A2 agonist, U46619 (100
490 nM)(Cauli et al., 2004) or K^+ enriched solution (composition in mM: 77.5 NaCl, 50 KCl, 1.25
491 NaH2PO4, 2 CaCl2, 1 MgCl2, 26 NaHCO3, 10 glucose, 15 sucrose). Vessels that did not constrict
492 with these applications were discarded. Only one arteriole was monitored per slice. IR-DGC
493 images were acquired at 0.1 Hz for pharmacological applications and at 1 Hz for optogenetic
494 experiments using Imaging Workbench 6.1 software (Indec Biosystems). The focal plane was
495 continuously maintained on-line using IR-DGC images of cells as anatomical landmarks
496 (Lacroix et al., 2015).

497 **Calcium imaging**

498 Visually and electrophysiologically identified layer II-III pyramidal cells were filled with the
499 calcium-sensitive dye Rhod-2 (200 µM, Cayman chemicals, 20777) using patch pipettes.
500 Optical recordings were made at least 15 min after passing in whole-cell configuration to allow
501 for somatic diffusion of the dye. Rhod-2 was excited with a 585 nm LED (Cool LED, Precise
502 Excite) at an intensity of 0.56 mW/mm² and the filter set used for optogenetic stimulation
503 using the Imaging Workbench 6.1 software (Indec Byosystems). IR-DGC and fluorescence
504 images were acquired by alternating epifluorescence and transmitted light sources. IR-DGC
505 and fluorescence were respectively sampled at 5 Hz and 1 Hz during baseline and optogenetic
506 stimulation, respectively, and at 1 Hz and 0.2 Hz after photostimulation. During
507 photostimulation, bleed-through occurred in the Rhod-2 channel due to the fluorescence of
508 the EYFP-ChR2 transgene(Madisen et al., 2012). Therefore, the Ca^{2+} response could not be
509 reliably analyzed during this period. To compensate for potential x-y drifts, all images were
510 registered off-line using the "StackReg" plug-in (Thévenaz et al., 1998) of the ImageJ 1.53
511 software. To define somatic regions of interest (ROIs), the soma was manually delineated from
512 IR-DGC images. Fluorescence intensity changes ($\Delta F/F_0$) were expressed as the ratio $(F-F_0)/F_0$
513 where F is the mean fluorescence intensity in the ROI at a given time point, and F_0 is the mean
514 fluorescence intensity in the same ROI during the 30-s control baseline.

515 **Drugs**

516 All pharmacological compounds were bath applied after a 5-min baseline, and vascular
517 dynamics were recorded during bath application. The following drugs were dissolved in water:
518 D-(-)-2-amino-5-phosphonopentanoic acid (D-AP5, 50 µM, Hellobio, HB0225), 6,7-
519 dinitroquinoxaline-2,3-dione (DNQX, 10µM, Hellobio, HB0262), LY367385 (100µM, Hellobio,
520 HB0398) and BIBP3226 (1 µM, Tocris, 2707). Tetrodotoxin (TTX, 1 µM, L8503, Latoxan) was
521 dissolved in 90 % acetic acid. PGE2 (HB3460, Hellobio), sulprostone (10 µM, Cayman chemical,
522 14765), 2-methyl-6-(phenylethynyl)pyridine (MPEP, 50 µM, Hellobio, HB0426) and 9,11-
523 dideoxy-9α,11α-methanoepoxy prostaglandin F2α (U-46619, 100 nM, Enzo, BML-PG023)
524 were dissolved in ethanol. Indomethacin (5 µM, Sigma-Aldrich, I7378), SC-560 (100 nM, Sigma-
525 Aldrich, S2064-5MG), NS-398 (10 µM, Enzo, BML-EI261), ONO-8130 (10 nM, Tocris, 5406), L-
526 798,106 (1 µM, Cayman chemical, 11129), AL8810 (10 µM, Cayman chemical, 16735), paxilline
527 (10 µM, Tocris, 2006) and HET0016 (100 µM, Merck, SML2416-5MG) in DMSO. Acetic acid,

528 ethanol and DMSO doses were always used below 0.1%. Synthesis inhibitors and BIBP3226
529 were applied at least 30 minutes before optogenetic stimulation. TTX was applied at least 15
530 minutes before, while glutamate receptor antagonists and paxilline were applied at least 10
531 and 5 minutes before, respectively.

532 **Vascular reactivity analysis**

533 To compensate for potential x-y drifts, all images were realigned off-line using the "StackReg"
534 plug-in (Thévenaz et al., 1998) of the ImageJ 1.53 software. Luminal diameter was measured
535 in layer I on registered images using custom analysis software developed in MATLAB
536 (MathWorks)(Lacroix et al., 2015). To avoid potential drawbacks due to vessel instability, only
537 arterioles with a stable diameter were analyzed further. Arterioles were considered stable if
538 the relative standard deviation of their diameter during the baseline period was less than
539 5%(Lacroix et al., 2015). Comparison of the mean arteriolar diameter during the 5-minute
540 baseline and the 5-minute final pharmacological treatments revealed that all drugs, except
541 AL8810, had no effect on resting diameter (Supplementary Fig. 4, 6 and 8).

542 Diameter changes ($\Delta D/D_0$) were expressed as $(D_t – D_0)/D_0$ where D_t is the diameter at the time
543 t and D_0 is the mean diameter during the baseline period. To eliminate sharp artifacts due to
544 transient loss of focus, diameter change traces were smoothed using a sliding three-point
545 median filter. The overall vascular response over time was captured by the area under the
546 curve of diameter changes after photostimulation. To determine the onset of
547 vasoconstriction, a Z-score was calculated from the diameter change traces using the formula:
548 $Z = (x - \mu)/ \sigma$, where both the mean μ and the standard deviation σ were calculated from the
549 values before photostimulation. Onset of vasoconstriction was defined as the time after the
550 start of photostimulation at which the Z-score exceeded or fell below -a value of -1.96 (95%
551 criteria) for 10 seconds. If a vessel showed no vasoconstriction, the onset was arbitrarily set
552 at 1800 seconds. Graphs were generated using R software version 4.3.0 (Team et al., 2023)
553 and Matplotlib package (Caswell et al., 2023).

554 **Intrinsic optical signals analysis**

555 Variations in IR light transmittance (ΔT)(Zhou et al., 2010) were determined using ImageJ 1.53
556 software according to: $\Delta T = (T_t - T_0)/ T_0$ where T_t is the light transmittance at a time t and T0 is
557 the average light transmittance during the baseline period of a squared region of interest of
558 100 µm x 100 µm manually delineated in layer I. The rate of ΔT change was determined as the

559 first derivative of ΔT (dΔT/dt, where ΔT is the change in light transmittance and t is time).
560 Slices that showed a maximum rate of increase of dΔT/dt greater than 2%/s, indicating the
561 occurrence of spreading depression (Zhou et al., 2010), were excluded.

562 **Surgery**

563 Chronic cranial windows were implanted one week after the head bar surgery as previously
564 described (Tournissac et al., 2022). We used a 100 µm thick glass coverslip over the barrel
565 cortex (~3mm^2). Before two-photon experiments, a recovery period of 7-10 days minimum
566 was maintained.

567 **Two-photon imaging and photostimulation**

568 For two-photon excitation, we used a femtosecond laser (Mai Tai eHP; SpectraPhysics) with a
569 dispersion compensation module (Deepsee; SpectraPhysics) emitting 70-fs pulses at 80 MHz.
570 The laser power was attenuated by an acousto-optical modulator (AA Optoelectronic, MT110-
571 B50-A1.5-IR-Hk). Scanning was performed with Galvanometric scanner (GS) mirrors
572 (8315KM60B; Cambridge Technology). Fluorescein was excited at 920 nm and the emitted
573 light was collected with a LUMFLN60XW (Olympus, 1.1 NA) water immersion objective.
574 Collected photons were sorted using a dichroic mirror centered at 570 nm, a FF01-525/25 nm
575 filter (Semrock) and a GaAsP (Hamamatsu) photomultipliers tube. Customized LabView
576 software was used to control the system. Line scans were drawn across pial vessels to measure
577 the change in arterioles diameter, which are less affected by potential movement in the x-y
578 plan than in penetrating arterioles, and whose dilation dynamics are similar in the
579 somatosensory cortex [14].

580 Mice were anesthetized with a mixture of ketamine and medetomidine (100 and 0.5 mg⁄kg,
581 respectively, intraperitoneal (i.p.)) during imaging sessions. Body temperature was
582 maintained at 36.5°C using a retro-controlled heating pad. Fluorescein dextran (70 kDa) was
583 injected i.v. through a retro-orbital injection to label brain vessels. Mice received continuous
584 air through a nose cone supplemented with oxygen to reach a final concentration of 30% O_2.
585 Photostimulation was delivered with a 473 nm laser (Coblot MLD, Sweden) through an optic
586 fiber placed above the glass coverslip and directed at the pial artery of interest. Each
587 photostimulation consisted of a 10-s train of 5 ms light pulses delivered at 10 Hz, respecting a
588 5 minutes interstimulus interval. Indomethacin (10mg/kg, #15425529, Thermo Fisher
589 Scientific) was administered i.v. through a retroorbital injection.

590 **Imaging analysis**

591 Pial arteriole diameter change was determined with line-scan acquisitions and a home-made
592 Matlab script as previously described (Rungta et al., 2018). Trials from the same vessel were
593 averaged (with a 0.1 s interpolation) for analysis. Area under the curve and statistics were
594 performed using GraphPad Prim (version 6).

595 **Cytoplasm harvesting and single-cell RT-PCR**

596 At the end of the whole-cell recording, which lasted less than 15 min, the cytoplasmic content
597 was collected in the recording pipette by applying a gentle negative pressure. The pipette's
598 content was expelled into a test tube and RT was performed in a final volume of 10 µl as
599 described previously (Devienne et al., 2018). The scRT-PCR protocol was designed to probed
600 simultaneously the expression of prostaglandins synthesizing enzymes and neuronal markers
601 (Lacroix et al., 2015). Prostaglandins synthesizing enzymes included COX-1 and COX-2, the
602 terminal PGE2 synthases (PGES): mPGES1, mPGES2 and cPGES, the terminal PGF2α synthases
603 (PGFS): PM-PGFS (Prxl2b) and AKR1B3 and the carbonyl reductase CBR1. Neuronal markers
604 included the vesicular glutamate transporter, vGluT1, and the two isoforms of glutamic acid
605 decarboxylase, GAD65 and GAD67. Two-step amplification was performed essentially as
606 described (Devienne et al., 2018). First, cDNAs present in the 10 µl reverse transcription
607 reaction were simultaneously amplified with all external primer pairs listed in Supplementary
608 table 2. Taq polymerase (2.5 U; Qiagen) and external primers mix (20 pmol each) were added
609 to the manufacturer's buffer (final volume, 100 µl), and 20 cycles (95◦C, 30 s; 60◦C, 30 s; and
610 72◦C, 35 s) of PCR were performed. Second rounds of PCR were performed using 1 µl of the
611 first PCR product as a template. In this second round, each cDNA was amplified individually
612 using its specific nested primer pair (Supplementary table 2) by performing 35 PCR cycles (as
613 described above). 10 µl of each individual PCR product were run on a 2% agarose gel stained
614 with ethidium bromide using ΦX174 digested by *HaeIII* as a molecular weight marker. The
615 efficiency of the protocol was validated using 500 pg of total forebrain RNAs (Supplementary
616 Fig. 5).

617 **Statistical analyses**

618 Statistical analyses were performed using GraphPad Prism version 7.00 for Windows
619 (GraphPad Software, La Jolla California USA, www.graphpad.com) and R software version
620 4.3.0 (Team et al., 2023). Normality of distribution was assessed using the Shapiro-Wilk tests.

621 Equality of variance was assessed using Brown-Forsythe tests for comparisons between
622 groups and using F-tests for comparisons with a control group. Parametric tests were only
623 used if these criteria were met. Statistical significance of morphological and physiological
624 properties of penetrating arterioles was determined using one-way ANOVA for comparison
625 between groups. Statistical significance of calcium was determined using two-tailed unpaired
626 t-tests and Statistical significance of vascular responses were appreciated using Tukey posthoc
627 tests for the different frequencies conditions and using Dunnett's posthoc tests for the
628 different pharmacological conditions compared to the 20 Hz condition without
629 pharmacological compound. False discovery rate correction was used for multiple
630 comparisons. Statistical significance of vascular diameter for drug applications was
631 determined using two-tailed paired t-tests. Statistical significance on all figures uses the
632 following convention: *$p<0.05$, **$p<0.01$ and ***$p<0.001$.

633 **Data availability statement**

634 The data that support the results of this study are available from the corresponding author
635 upon reasonable request.

636 **Acknowledgements**

637 The authors thank Dr Rebecca Piskorowski for constructive criticism of the manuscript. We
638 acknowledge the invaluable support of the animal facilities of IBPS (RongIBPS) and Institut de
639 la vision for their expert care and maintenance of the animals used in this study. Financial
640 support was provided by grants from the Agence Nationale pour la Recherche (ANR-17-CE37-
641 0010-03, B.C.; CE37_2020_TF-fUS-CADASIL, S.C.; ANR-20-CE14-0025, D.L.; ANR-23-CE14-
642 0038-01, B.C.), the Fondation Alzheimer France (M21JRCN009, S.C.) and the i-Bio initiative of
643 Sorbonne University (B.C.). B.L.G. and E.B. were supported by fellowships from Fondation pour
644 la Recherche sur Alzheimer and M.T. by a fellowship from the Fondation pour la Recherche
645 Médicale (SPF201909009103).

646 **Author contributions**

647 B.L.G., M.T., and E.B. designed experiments, acquired, and analyzed the data, and edited the
648 manuscript. S.P. acquired the data. B.L.G. and B.C. drafted the manuscript. I.D. edited the
649 manuscript. H.S. analyzed the data. D.L. designed experiments and edited the manuscript. S.C.
650 and B.C. designed experiments and edited the manuscript.

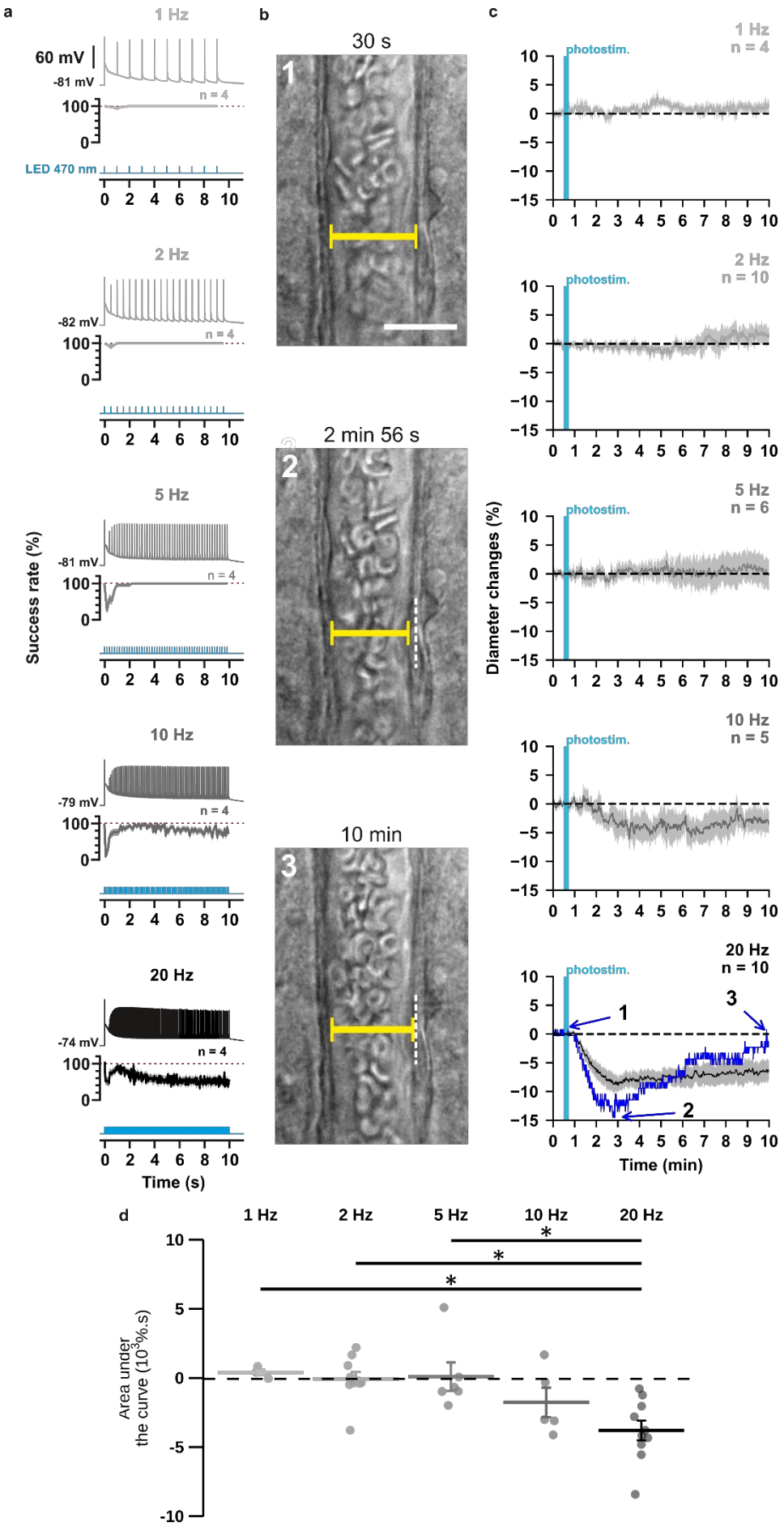
a
1 Hz
60 mV
-81 mV
n = 4
100
0
LED 470 nm
0 2 4 6 8 10
2 Hz
-82 mV
n = 4
5 Hz
-81 mV
n = 4
10 Hz
-79 mV
n = 4
20 Hz
-74 mV
n = 4
Success rate (%)
Time (s)
b
30 s
1
2 min 56 s
2
10 min
3
c
photostim.
1 Hz
n = 4
2 Hz
n = 10
5 Hz
n = 6
10 Hz
n = 5
20 Hz
n = 10
Diameter changes (%)
Time (min)
d
1 Hz
2 Hz
5 Hz
10 Hz
20 Hz
Area under the curve (10^-3%.s)

Figure 1: The occurrence and strength of vasoconstriction depends on the photostimulation frequency of pyramidal cells. (a) Representative examples of the voltage responses of a layer II-III pyramidal cell (upper traces light grey to black traces) induced by photostimulations (470 nm, 10 s train, 5 ms pulses) delivered at 1, 2, 5, 10 and 20 Hz (cyan lower traces) and mean spike success rate (middle trace, n= 4 cells from 3 mice). The SEMs envelope the mean traces. The red dashed lines represent a spike success rate of 100%. **(b)** Representative example showing IR-DGC pictures of a layer I penetrating arteriole (1) before a 20 Hz photostimulation, (2) at the maximal diameter decrease, and (3) after 10 minutes of recording. Pial surface is upward. Yellow calipers represent the measured diameters. White dashed lines indicate the initial position of the vessel wall. Scale bar: 25 µm. **(c)** Kinetics of arteriolar diameter changes induced by photostimulation (vertical cyan bars) at 1 Hz (n= 4 arterioles from 3 mice), 2 Hz (n= 10 arterioles from 8 mice), 5 Hz (n= 6 arterioles from 6 mice), 10 Hz (n= 5 arterioles from 5 mice) and 20 Hz (n= 10 arteriole from 9 mice). The SEMs envelope the mean traces. The blue trace represents the kinetics of the diameter changes of the arteriole shown in (b). **(d)** Effects of the different photostimulation frequencies on AUC of vascular responses during 10 min of recording. Data are presented as the individual values and mean ± SEM. * statistically different from 20 Hz stimulation with $p<0.05$.

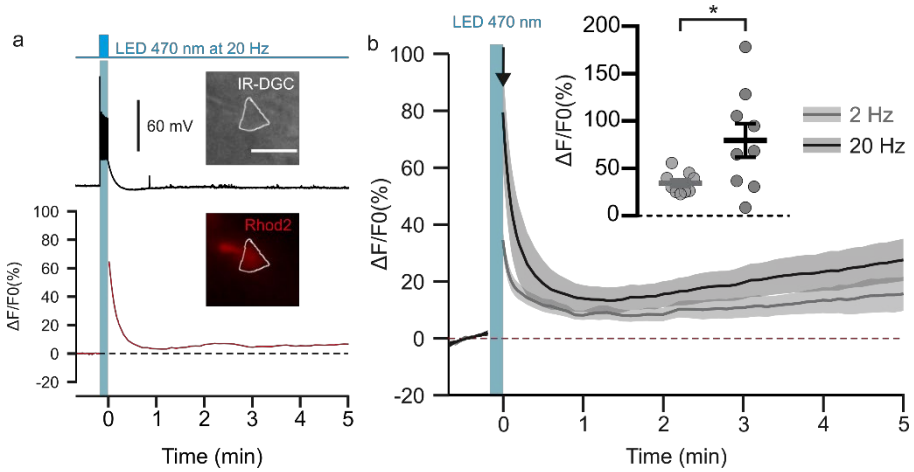

Figure 2: Photostimulation of pyramidal cells elicits a time-locked firing and a frequency-dependent calcium increase. (**a**). Voltage response (top trace) and kinetics of relative fluorescence changes (red bottom trace) induced by photostimulation at 20 Hz. Insets, IR-DGC (top), Rhod2 fluorescence (bottom) pictures of an imaged layer II/III pyramidal cell. The somatic region of interest is outlined in white. Pial surface is upward. Scale bar: 20 µm. **(b)** Mean relative variations of Ca^{2+} fluorescence in response to photostimulation at 2 Hz (grey) and 20 Hz (black). Dashed line represents the baseline. The vertical cyan bar indicates the duration of photostimulation. SEMs envelope the mean traces. Inset, Maximum increase in relative fluorescence changes induced immediately after photostimulation, indicated by the black arrow. The data are shown as the individual values and mean ± SEM. * statistically different with $p < 0.05$.

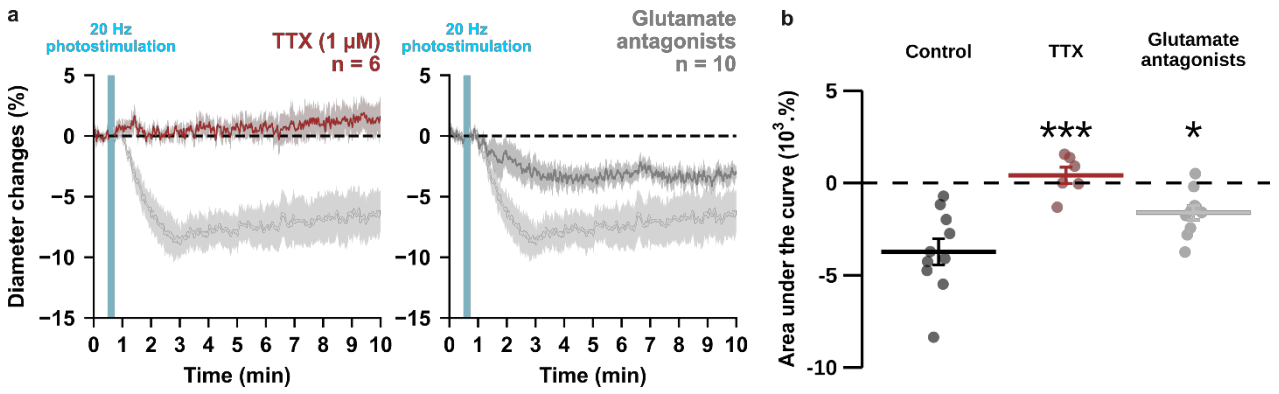

Figure 3: Optogenetically-induced vasoconstriction requires AP firing and partially glutamatergic transmission. Effect of TTX (1 µM, brown, n= 6 arterioles from 5 mice) and cocktail antagonists of AMPA/kainate (DNQX, 10 µM), NMDA (D-AP5, 50 µM), mGluR1 (LY367385, 100 µM) and mGluR5 (MPEP, 50 µM) receptors (gray, n= 10 arterioles from 6 mice) on **(a)** kinetics and **(b)** magnitude of arteriolar vasoconstriction induced by 20 Hz photostimulation (cyan bar). The SEMs envelope the mean traces. Dashed lines represent the initial diameter. The shaded traces correspond to the kinetics of arteriolar vasoconstriction in control condition (Fig. 1c – 20 Hz). Data are presented as the individual values and mean ± SEM. * and *** statistically different from control condition (Fig. 1c – 20 Hz) with $p<0.05$ and $p<0.001$, respectively.

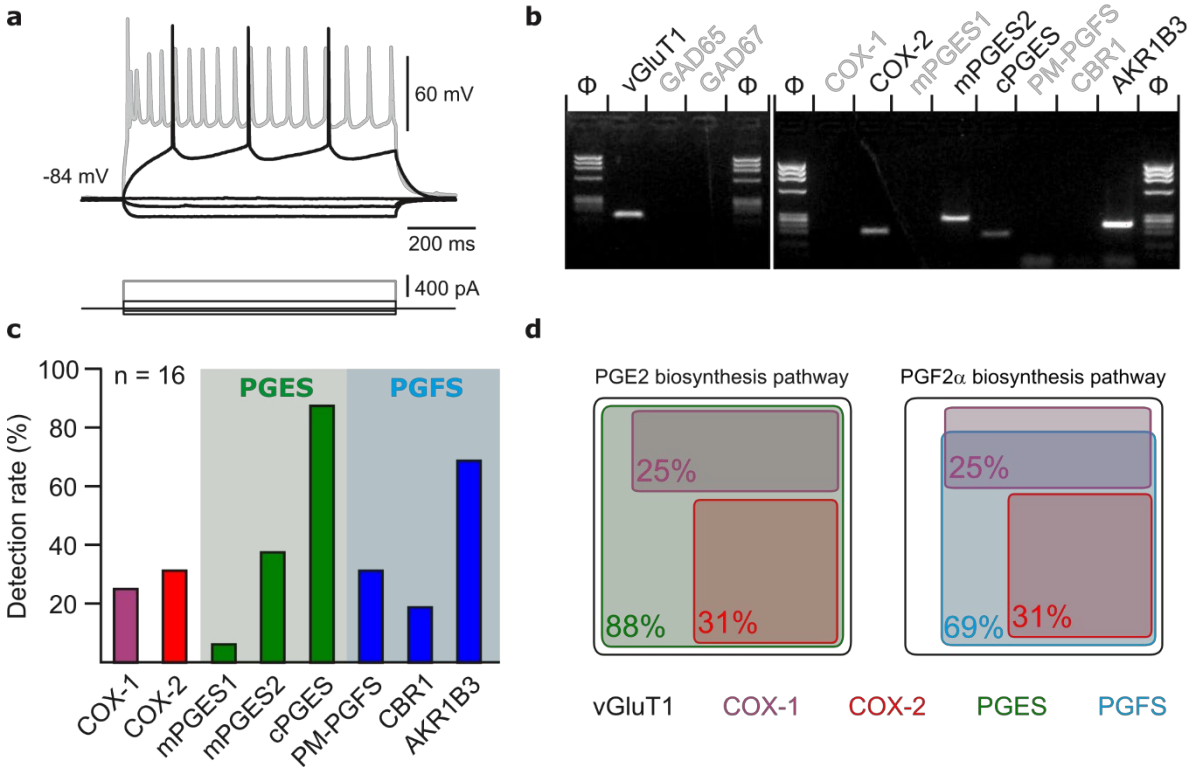

Figure 4: Layer II-III pyramidal cells express PGE2 and PGF2α synthesizing enzymes. (a) Voltage responses of a layer II-III pyramidal cell induced by injection of current (bottom traces). In response to a just-above-threshold current pulse, the neuron fired long-lasting action potentials with little frequency adaptation (middle black trace). Near saturation, it exhibits the pronounced spike amplitude accommodation and marked frequency adaptation characteristic of regular spiking cells (upper grey trace). **(b)** Agarose gel analysis of the scRT-PCR products of the pyramidal cell shown in (**a**) revealing expression of vGluT1, COX-2, mPGES2, cPGES, PM-PGFS and CBR1. Φx174 digested by *HaeIII* (Φ) was used as molecular weight marker **(c)** Histogram summarizing the single-cell detection rate of PGE2 and PGf2α synthesizing enzymes in layer II-III pyramidal cells (n= 16 cells from 6 mice). PGES (green zone) corresponds to mPGES1, mPGES2 and/or cPGES and PGFS (blue zone) to PM-PGFS, CBR1 and/or AKR1B3. **(d)** Co-expression of PGE2 and PGf2α synthesizing enzymes in pyramidal cells. The box size is proportional to the detection rate. Note the absence of co-expression between COX-1 (purple) and COX-2 (red). Co-expression of a PGES (left, green) and a PGFS (right, blue) with COX-1 (up) and COX-2 (bottom).

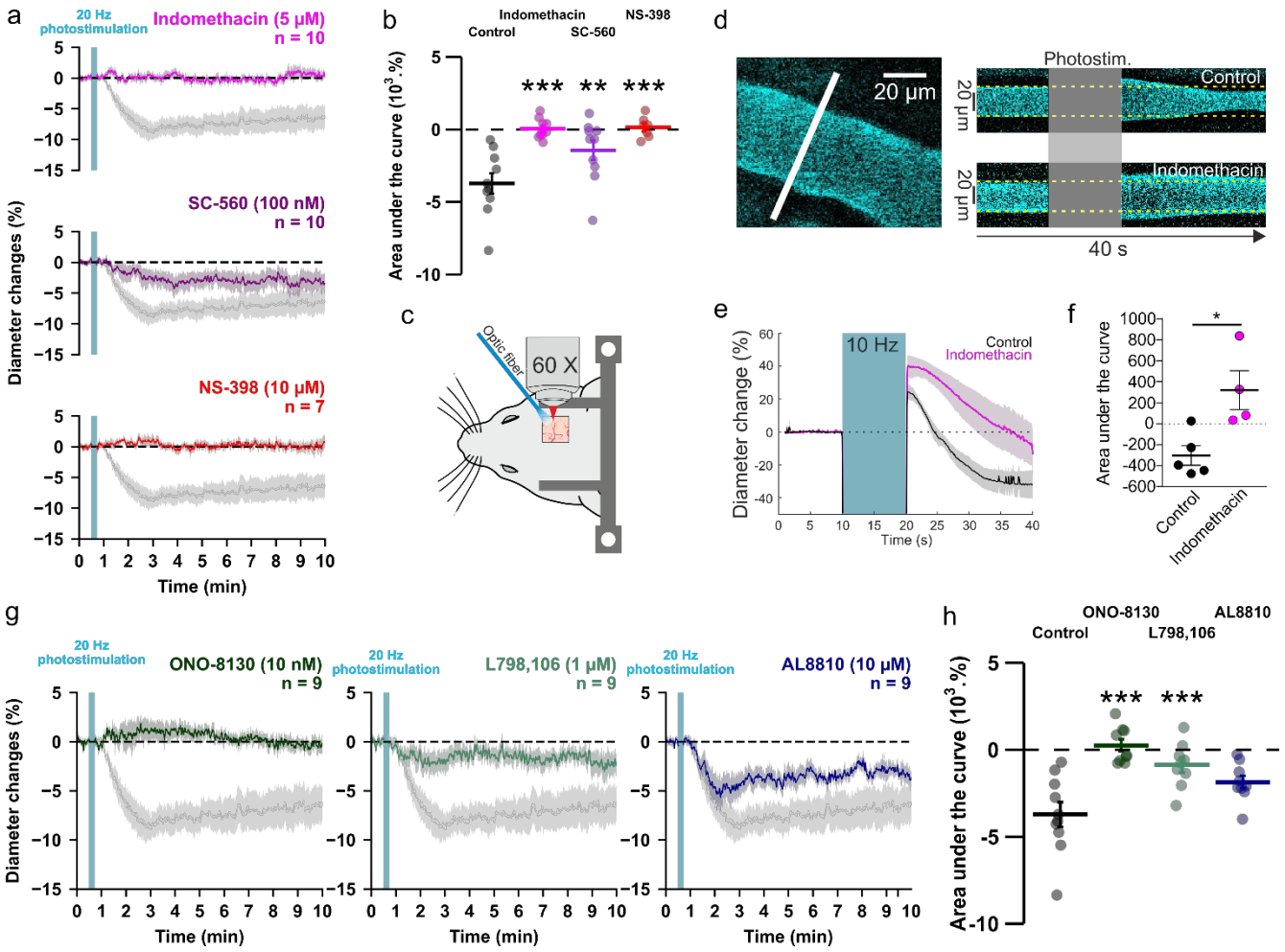
a
20 Hz photostimulation
Indomethacin (5 μM)
n = 10
SC-560 (100 nM)
n = 10
NS-398 (10 μM)
n = 7
Diameter changes (%)
Time (min)
b
Control
Indomethacin
SC-560
NS-398
Area under the curve (10³.%)
***
**
***
c
Optic fiber
60 X
d
20 μm
Photostim.
Control
Indomethacin
20 μm
20 μm
40 s
e
10 Hz
Control
Indomethacin
Diameter change (%)
Time (s)
f
Area under the curve
*
Control
Indomethacin
g
20 Hz photostimulation
ONO-8130 (10 nM)
n = 9
L798,106 (1 μM)
n = 9
AL8810 (10 μM)
n = 9
Diameter changes (%)
Time (min)
h
Control
ONO-8130
L798,106
AL8810
Area under the curve (10³.%)
***
***

Figure 5: PGE2 mostly derived from COX-2 activity and its EP1 and EP3 receptors mediates vasoconstriction induced by optogenetically activated pyramidal cells. (a, b) *Ex vivo* effects of the COX1/2 inhibitor indomethacin (magenta, n= 10 arterioles from 9 mice), the COX-1 inhibitor SC-560 (purple, n= 10 arterioles from 7 mice), and the COX-2 inhibitor NS-398 (red, n= 7 arterioles from 6 mice) on kinetics **(a)** and AUC **(b)** of arteriolar vasoconstriction induced by 20 Hz photostimulation (vertical cyan bar). **(c)** Optogenetic stimulation was achieved *in vivo* with an optic fiber through a chronic cranial window over the barrel cortex. **(d)** Left, diameter of pial arterioles labeled with fluorescein dextran (i.v) was measured with line-scan crossing the vessel (white line). Right, Representative examples of vascular response upon photostimulation (10 Hz, 10 s) under control (top) and indomethacin condition (bottom). **(e)** Diameter changes upon photostimulation under control (black; n = 5 arterioles, 4 mice) or indomethacin (magenta; n = 4 arterioles, 4 mice) conditions. **(f)** Area under the curve of the diameter change in control (black) or indomethacin (magenta) conditions calculated between 20 and 40 s (unpaired, two-tailed Mann Whitney test, * $p<0.05$). **(g, h)** Effects of the EP1, EP3 and FP antagonists, ONO-8130 (10 nM, dark green, n= 9 arterioles from 7 mice), L798,106 (1 µM, light green, n= 9 arterioles from 5 mice) and AL8810 (10 µM, dark blue, n= 9 arterioles from 7 mice), respectively, on kinetics **(g)** and AUC **(h)** of arteriolar vasoconstriction induced by 20 Hz photostimulation. The data are shown as the individual values and mean ± SEM. Dashed line represents the baseline. The SEMs envelope the mean traces. The data are shown as the individual values and mean ± SEM. The shaded traces correspond to the control condition (Fig. 1c – 20 Hz). *, ** and *** statistically different from 20 Hz control condition with $p< 0.05$, 0.01 and 0.001, respectively.

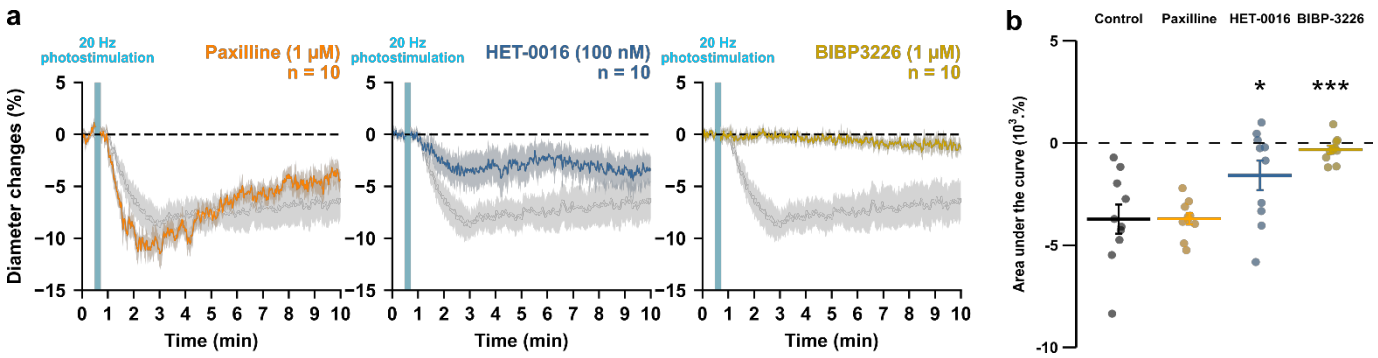

Figure 6: NPY Y1 receptors activation and 20-HETE synthesis mediates the vasoconstriction induced by pyramidal neurons. Effects of paxilline (1 µM, orange, n= 10 arterioles from 6 mice), HET-0016 (100 nM, blue-grey, n= 10 arterioles from 7 mice) and BIBP3226 (1 µM, yellow, n= 10 arterioles from 6 mice) on **(a)** kinetics and **(b)** AUC of arteriolar vasoconstriction induced by 20 Hz photostimulation (vertical blue bar). Dashed line represents the baseline. The SEMs envelope the mean traces. The shaded traces correspond to the control condition (Fig. 1c – 20 Hz). The data are shown as the individual values and mean ± SEM. * and *** statistically different from 20 Hz control condition with $p < 0.05$ and 0.001.

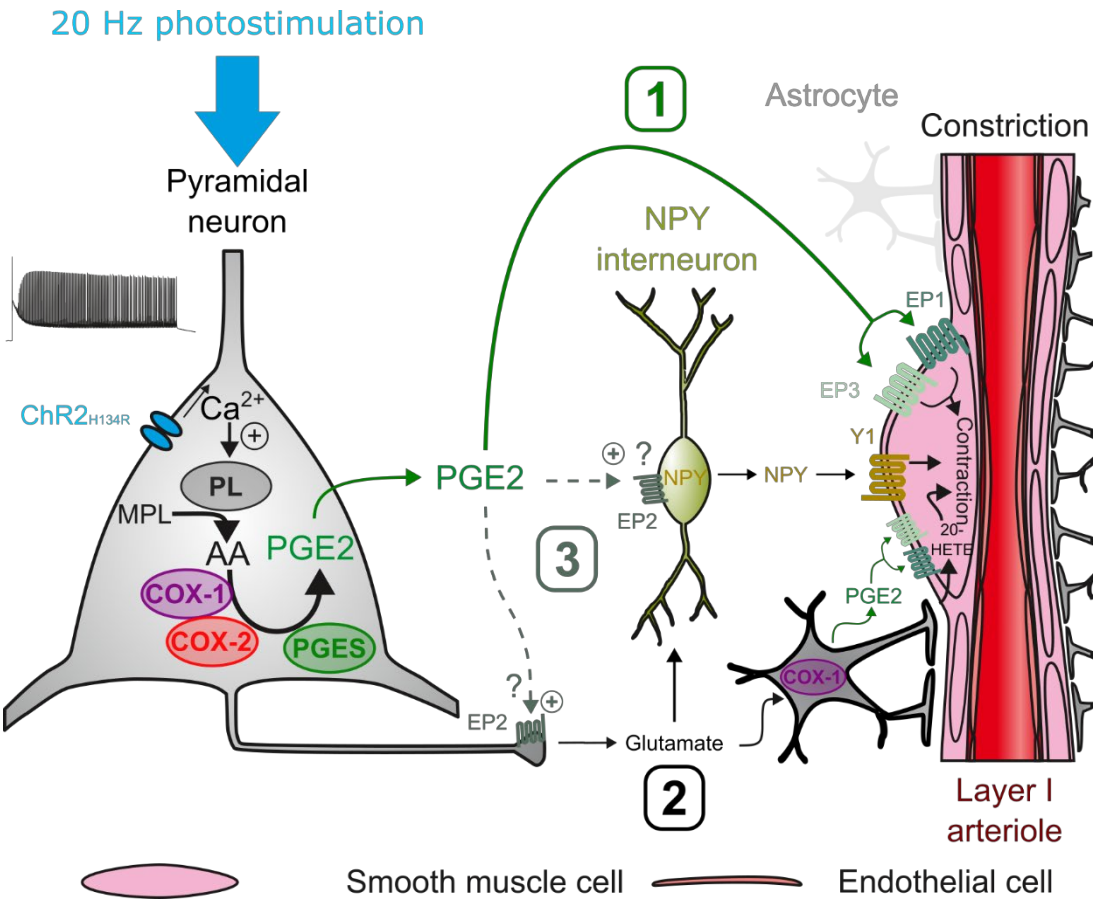

Figure 7: Possible pathways of vasoconstriction induced by pyramidal neurons. 20 Hz photostimulation induces activation of pyramidal neurons expressing channelrhodopsin-2 ($ChR2_{H134R}$) and increases intracellular calcium (Ca^{2+}). Arachidonic acid (AA) is released from membrane phospholipids (MPL) by phospholipases (PL) activated by intracellular Ca^{2+} and is metabolized by type-1 and type-2 cyclooxygenases (COX-1 and COX-2) and prostaglandin E2 synthases (PGES) to produce prostaglandin E2 (PGE2). Three non-exclusive pathways can be proposed for arteriolar vasoconstriction in layer I: 1) PGE2 released into the extracellular space may act directly on arteriolar EP1 and EP3 receptors to induce smooth muscle cell constriction. 2) Glutamate released from pyramidal cells may activate neuropeptide Y (NPY) interneurons and NPY is released to act on Y1 receptors to constrict smooth muscle cells. Glutamate can also activate astrocytes to induce constriction through the 20-HETE and the COX-1/PGE2 pathways. 3) PGE2 may act on pre- and postsynaptic EP2 receptors to facilitate glutamate release and NPY interneuron activation, respectively.

References

651 Alix E, Schmitt C, Strazielle N, Ghersi-Egea JF. 2008. Prostaglandin E2 metabolism in rat brain:
652 Role of the blood-brain interfaces. *Cerebrospinal Fluid Res* **5**. doi:10.1186/1743-8454-5-5

653 Asadi-Pooya AA, Sperling MR. 2019. Normal Awake, Drowsy, and Sleep EEG Patterns That
654 Might Be Overinterpreted as Abnormal. *Journal of Clinical Neurophysiology*.
655 doi:10.1097/WNP.0000000000000585

656 Attwell D, Buchan AM, Charpak S, Lauritzen M, Macvicar BA, Newman EA. 2010. Glial and
657 neuronal control of brain blood flow. *Nature* **468**:232–243. doi:10.1038/nature09613

658 Attwell D, Mishra A, Hall CN, O'Farrell FM, Dalkara T. 2016. What is a pericyte? *Journal of*
659 *Cerebral Blood Flow and Metabolism* **36**:451–455. doi:10.1177/0271678X15610340

660 Baraban SC. 2004. Neuropeptide Y and epilepsy: Recent progress, prospects and
661 controversies. *Neuropeptides*. doi:10.1016/j.npep.2004.04.006

662 Bezzina C, Verret L, Juan C, Remaud J, Halley H, Rampon C, Dahan L. 2015. Early onset of
663 hypersynchronous network activity and expression of a marker of chronic seizures in the
664 Tg2576 mouse model of Alzheimer's disease. *PLoS One* **10**.
665 doi:10.1371/journal.pone.0119910

666 Blanco M, Stern JE, Filosa JA. 2008. Tone-dependent vascular responses to astrocyte-derived
667 signals. *American journal of physiology* 2855–2863. doi:10.1152/ajpheart.91451.2007.

668 Boie Y, Stocco R, Sawyer N, Slipetz DM, Ungrin MD, Neuschafer-rube F, Puschel GP. 1997.
669 Molecular cloning and characterization of the four rat prostaglandin E 2 prostanoid
670 receptor subtypes 227–241.

671 Caswell TA, Andrade ES de, Lee A, Droettboom M, Hoffmann T, Klymak J, Hunter J, Firing E,
672 Stansby D, Varoquaux N, Nielsen JH, Gustafsson O, Root B, May R, Elson P, Seppänen JK,
673 Lee J-J, Dale D, Sunden K, hannah, McDougall D, Straw A, Hobson P, Lucas G, Gohlke C,
674 Vincent AF, Yu TS, Ma E, Silvester S, Moad C. 2023. matplotlib/matplotlib: REL: v3.7.2.
675 doi:10.5281/ZENODO.8118151

676 Cauli B, Hamel E. 2010. Revisiting the role of neurons in neurovascular coupling. *Front*
677 *Neuroenergetics* **2**:9. doi:10.3389/fnene.2010.00009

678 Cauli B, Tong XK, Rancillac A, Serluca N, Lambolez B, Rossier J, Hamel E. 2004. Cortical GABA
679 interneurons in neurovascular coupling: Relays for subcortical vasoactive pathways.
680 *Journal of Neuroscience* **24**:8940–8949. doi:10.1523/JNEUROSCI.3065-04.2004

681 Chaudhry UA, Zhuang H, Crain BJ, Doré S. 2008. Elevated microsomal prostaglandin-E
682 synthase-1 in Alzheimer's disease. *Alzheimer's and Dementia* **4**:6–13.
683 doi:10.1016/j.jalz.2007.10.015

684 Chung DY, Sadeghian H, Qin T, Lule S, Lee H, Karakaya F, Goins S, Oka F, Yaseen MA, Houben
685 T, Tolner EA, Van Den Maagdenberg AMJMJMJM, Whalen MJ, Sakadžić S, Ayata C. 2018.
686 Determinants of Optogenetic Cortical Spreading Depolarizations. *Cerebral Cortex* **29**:1–
687 12. doi:10.1093/cercor/bhy021

688 Clasadonte J, Poulain P, Hanchate NK, Corfas G, Ojeda SR, Prevot V. 2011. Prostaglandin E 2
689 release from astrocytes triggers gonadotropin-releasing hormone (GnRH) neuron firing
690 via EP2 receptor activation. *Proc Natl Acad Sci U S A* **108**:16104–16109.
691 doi:10.1073/pnas.1107533108

692 Dabertrand F, Hannah RM, Pearson JM, Hill-Eubanks DC, Brayden JE, Nelson MT. 2013.
693 Prostaglandin E2, a postulated astrocyte-derived neurovascular coupling agent,
694 constricts rather than dilates parenchymal arterioles. *Journal of Cerebral Blood Flow and*
695 *Metabolism* **33**:479–482. doi:10.1038/jcbfm.2013.9

696 Desai S, April H, Nwaneshiudu C, Ashby B. 2000. Comparison of agonist-induced internalization
697 of the human EP2 and EP4 prostaglandin receptors: Role of the carboxyl terminus in EP4
698 receptor sequestration. *Mol Pharmacol* **58**:1279–1286. doi:10.1124/mol.58.6.1279

699 Devienne G, Le Gac B, Piquet J, Cauli B. 2018. Single Cell Multiplex Reverse Transcription
700 Polymerase Chain Reaction After Patch-Clamp. *Journal of Visualized Experiments* **136**:1–
701 12. doi:10.3791/57627

702 Devor A, Hillman EMC, Tian P, Waeber C, Teng IC, Ruvinskaya L, Shalinsky MH, Zhu H, Haslinger
703 RH, Narayanan SN, Ulbert I, Dunn AK, Lo EH, Rosen BR, Dale AM, Kleinfeld D, Boas DA.
704 2008. Stimulus-Induced Changes in Blood Flow and 2-Deoxyglucose Uptake Dissociate in
705 Ipsilateral Somatosensory Cortex. *Journal of Neuroscience* **28**:14347–14357.
706 doi:10.1523/JNEUROSCI.4307-08.2008

707 Devor A, Tian P, Nishimura N, Teng IC, Hillman EMC, Narayanan SN, Ulbert I, Boas DA, Kleinfeld
708 D, Dale AM. 2007. Suppressed Neuronal Activity and Concurrent Arteriolar
709 Vasoconstriction May Explain Negative Blood Oxygenation Level-Dependent Signal.
710 *Journal of Neuroscience* **27**:4452–4459. doi:10.1523/JNEUROSCI.0134-07.2007

711 Di Cesare A, Del Piccolo P, Zacchetti D, Grohovaz F. 2006. EP2 receptor stimulation promotes
712 calcium responses in astrocytes via activation of the adenylyl cyclase pathway. *Cellular*
713 *and Molecular Life Sciences* **63**:2546–2553. doi:10.1007/s00018-006-6262-9

714 Farrell JS, Gaxiola-Valdez I, Wolff MD, David LS, Dika HI, Geeraert BL, Wang R, Singh S,
715 Spanswick SC, Dunn JF, Antle MC, Federico P, Campbell Teskey G. 2016. Postictal
716 behavioural impairments are due to a severe prolonged hypoperfusion/ hypoxia event
717 that is COX-2 dependent. doi:10.7554/eLife.19352.001

718 Gicquiaux H, Lecat S, Gaire M, Dieterlen A, Mély Y, Takeda K, Bucher B, Galzi JL. 2003.
719 Neuropeptide Y-induced contraction and its desensitization through the neuropeptide Y
720 receptor subtype in several rat veins. *J Cardiovasc Pharmacol* **41 Suppl 1**:S23-7.

721 Gicquiaux H, Lecat S, Gaire M, Dieterlen A, Mély Y, Takeda K, Bucher B, Galzi JL. 2002. Rapid
722 internalization and recycling of the human neuropeptide Y Y1 receptor. *Journal of*
723 *Biological Chemistry* **277**:6645–6655. doi:10.1074/jbc.M107224200

724 Girouard H, Bonev AD, Hannah RM, Meredith A, Aldrich RW, Nelson MT. 2010. Astrocytic
725 endfoot Ca2+ and BK channels determine both arteriolar dilation and constriction. *Proc*
726 *Natl Acad Sci U S A* **107**:3811–3816. doi:10.1073/pnas.0914722107

727 Gordon GRJ, Choi HB, Rungta RL, Ellis-Davies GCR, MacVicar BA. 2008. Brain metabolism
728 dictates the polarity of astrocyte control over arterioles. *Nature* **456**:745–9.
729 doi:10.1038/nature07525

730 Gorski JA, Talley T, Qiu M, Puelles L, Rubenstein JLRR, Jones KR. 2002. Cortical excitatory
731 neurons and glia, but not GABAergic neurons, are produced in the Emx1-expressing
732 lineage. *Journal of Neuroscience* **22**:6309–6314. doi:10.1523/jneurosci.22-15-
733 06309.2002

734 Hartmann DA, Berthiaume AA, Grant RI, Harrill SA, Koski T, Tieu T, McDowell KP, Faino A V.,
735 Kelly AL, Shih AY. 2021. Brain capillary pericytes exert a substantial but slow influence on
736 blood flow. *Nat Neurosci* **24**:633–645. doi:10.1038/s41593-020-00793-2

737 Hill RA, Tong L, Yuan P, Murikinati S, Gupta S, Grutzendler J. 2015. Regional Blood Flow in the
738 Normal and Ischemic Brain Is Controlled by Arteriolar Smooth Muscle Cell Contractility
739 and Not by Capillary Pericytes. *Neuron* **87**:95–110. doi:10.1016/j.neuron.2015.06.001

740 Iadecola C. 2017. The Neurovascular Unit Coming of Age: A Journey through Neurovascular
741 Coupling in Health and Disease. *Neuron* **96**:17–42. doi:10.1016/j.neuron.2017.07.030

742 Jiruska P, de Curtis M, Jefferys JGR, Schevon CA, Schiff SJ, Schindler K. 2013. Synchronization
743 and desynchronization in epilepsy: Controversies and hypotheses. *Journal of Physiology*.
744 doi:10.1113/jphysiol.2012.239590

745 Kahn I, Knoblich U, Desai M, Bernstein J, Graybiel AM, Boyden ES, Buckner RL, Moore CI. 2013.
746 Optogenetic drive of neocortical pyramidal neurons generates fMRI signals that are
747 correlated with spiking activity. *Brain Res* **1511**:33–45.
748 doi:10.1016/j.brainres.2013.03.011

749 Karagiannis A, Gallopin T, Dávid C, Battaglia D, Geoffroy H, Rossier J, Hillman EMC, Staiger JF,
750 Cauli B. 2009. Classification of NPY-expressing neocortical interneurons. *J Neurosci*
751 **29**:3642–59. doi:10.1523/JNEUROSCI.0058-09.2009

752 Kasischke KA, Lambert EM, Panepento B, Sun A, Gelbard HA, Burgess RW, Foster TH,
753 Nedergaard M. 2011. Two-photon NADH imaging exposes boundaries of oxygen diffusion
754 in cortical vascular supply regions. *Journal of Cerebral Blood Flow and Metabolism* **31**:68–
755 81. doi:10.1038/jcbfm.2010.158

756 Krawchuk MB, Ruff CF, Yang X, Ross SE, Vazquez AL. 2020. Optogenetic assessment of VIP, PV,
757 SOM and NOS inhibitory neuron activity and cerebral blood flow regulation in mouse
758 somato-sensory cortex. *Journal of Cerebral Blood Flow and Metabolism* **40**:1427–1440.
759 doi:10.1177/0271678X19870105

760 Lacroix A, Toussay X, Anenberg E, Lecrux C, Ferreirós N, Karagiannis A, Plaisier F, Chausson P,
761 Jarlier F, Burgess SA, Hillman EMCCC, Tegeder I, Murphy TH, Hamel E, Cauli B, Ferreiro N,
762 Burgess SA, Hillman EMCCC, Tegeder I, Murphy TH, Hamel E, Cauli B. 2015. COX-2-

763 Derived Prostaglandin E2 Produced by Pyramidal Neurons Contributes to Neurovascular
764 Coupling in the Rodent Cerebral Cortex. *J Neurosci* **35**:11791–11810.
765 doi:10.1523/JNEUROSCI.0651-15.2015

766 Lecrux C, Toussay X, Kocharyan A, Fernandes P, Neupane S, Levesque M, Plaisier F, Shmuel A,
767 Cauli B, Hamel E. 2011. Pyramidal Neurons Are "Neurogenic Hubs" in the Neurovascular
768 Coupling Response to Whisker Stimulation. *Journal of Neuroscience* **31**:9836–9847.
769 doi:10.1523/JNEUROSCI.4943-10.2011

770 Lee JMJ, Stile CL, Bice AR, Rosenthal ZP, Yan P, Snyder AZ, Lee JMJ, Bauer AQ. 2020. Opposed
771 hemodynamic responses following increased excitation and parvalbumin-based
772 inhibition. *Journal of Cerebral Blood Flow and Metabolism*.
773 doi:10.1177/0271678X20930831

774 Lin JY, Lin MZ, Steinbach P, Tsien RY. 2009. Characterization of engineered channelrhodopsin
775 variants with improved properties and kinetics. *Biophys J* **96**:1803–1814.
776 doi:10.1016/j.bpj.2008.11.034

777 Ma Y, Shaik MA, Kozberg MG, Kim SH, Portes JP, Timerman D. 2016. Resting-state
778 hemodynamics are spatiotemporally coupled to synchronized and symmetric neural
779 activity in excitatory neurons. *Proceedings of the National Academy of Sciences*.
780 doi:10.1073/pnas.1525369113

781 Madisen L, Mao T, Koch H, Zhuo J, Berenyi A, Fujisawa S, Hsu Y-W a, Garcia AJ, Gu X, Zanella
782 S, Kidney J, Gu H, Mao Y, Hooks BM, Boyden ES, Buzsáki G, Ramirez JM, Jones AR, Svoboda
783 K, Han X, Turner EE, Zeng H. 2012. A toolbox of Cre-dependent optogenetic transgenic
784 mice for light-induced activation and silencing. *Nat Neurosci* **15**:793–802.
785 doi:10.1038/nn.3078

786 Mishra A, Reynolds JP, Chen Y, Gourine A V., Rusakov DA, Attwell D. 2016. Astrocytes mediate
787 neurovascular signaling to capillary pericytes but not to arterioles. *Nat Neurosci* **19**:1619–
788 1627. doi:10.1038/nn.4428

789 Mulligan SJ, MacVicar BA. 2004. Calcium transients in astrocyte endfeet cause cerebrovascular
790 constrictions. *Nature* **431**:195–199. doi:10.1038/nature02827

791 Niwa K, Araki E, Morham SG, Ross ME, Iadecola C. 2000. Cyclooxygenase-2 contributes to
792 functional hyperemia in whisker-barrel cortex. *Journal of Neuroscience* **20**:763–770.
793 doi:10.1523/jneurosci.20-02-00763.2000

794 O'Herron P, Chhatbar PY, Levy M, Shen Z, Schramm AE, Lu Z, Kara P. 2016. Neural correlates
795 of single-vessel haemodynamic responses in vivo. *Nature* **534**:378–382.
796 doi:10.1038/nature17965

797 Palop JJ, Chin J, Roberson ED, Wang J, Thwin MT, Bien-Ly N, Yoo J, Ho KO, Yu GQ, Kreitzer A,
798 Finkbeiner S, Noebels JL, Mucke L. 2007. Aberrant Excitatory Neuronal Activity and
799 Compensatory Remodeling of Inhibitory Hippocampal Circuits in Mouse Models of
800 Alzheimer's Disease. *Neuron* **55**:697–711. doi:10.1016/j.neuron.2007.07.025

801 Palop JJ, Mucke L. 2010. Amyloid-B-induced neuronal dysfunction in Alzheimer's disease:
802 From synapses toward neural networks. *Nat Neurosci* **13**:812–818. doi:10.1038/nn.2583

803 Pasinetti GM, Aisen PS. 1998. Cyclooxygenase-2 expression is increased in frontal cortex of
804 Alzheimer's disease brain. *Neuroscience* **87**:319–324. doi:10.1016/S0306-
805 4522(98)00218-8

806 Rancillac A, Rossier J, Guille M, Tong X-K, Geoffroy H, Amatore C, Arbault S, Hamel E, Cauli B.
807 2006. Glutamatergic Control of Microvascular Tone by Distinct GABA Neurons in the
808 Cerebellum. *J Neurosci* **26**:6997–7006. doi:10.1523/JNEUROSCI.5515-05.2006

809 Rosehart AC, Longden TA, Weir N, Fontaine JT, Joutel A, Dabertrand F. 2021. Prostaglandin E2
810 Dilates Intracerebral Arterioles When Applied to Capillaries: Implications for Small Vessel
811 Diseases. *Front Aging Neurosci* **13**:1–11. doi:10.3389/fnagi.2021.695965

812 Rungta RL, Chaigneau E, Osmanski BF, Charpak S. 2018. Vascular Compartmentalization of
813 Functional Hyperemia from the Synapse to the Pia. *Neuron* 1–14.
814 doi:10.1016/j.neuron.2018.06.012

815 Rungta RL, Osmanski B-F, Boido D, Tanter M, Charpak S. 2017. Light controls cerebral blood
816 flow in naive animals. *Nat Commun* **8**:14191. doi:10.1038/ncomms14191

817 Rungta RL, Zuend M, Aydin A, Weber B, Charpak S, Boido D. 2021. vascular arbors in layer II /
818 III somatosensory cortex. *Commun Biol*. doi:10.1038/s42003-021-02382-w

819 Sang N, Zhang J, Marcheselli V, Bazan NG, Chen C. 2005. Postsynaptically Synthesized
820 Prostaglandin E2 (PGE2) Modulates Hippocampal Synaptic Transmission via a Presynaptic
821 PGE2 EP2 Receptor. *Journal of Neuroscience* **25**:9858–9870.
822 doi:10.1523/JNEUROSCI.2392-05.2005

823 Schmid F, Barrett MJPP, Jenny P, Weber B. 2019. Vascular density and distribution in
824 neocortex. *Neuroimage* **197**:792–805. doi:10.1016/j.neuroimage.2017.06.046

825 Scott NA, Murphy TH. 2012. Hemodynamic responses evoked by neuronal stimulation via
826 channelrhodopsin-2 can be independent of intracortical glutamatergic synaptic
827 transmission. *PLoS One* **7**:1–10. doi:10.1371/journal.pone.0029859

828 Sharif NA, Klimko PG. 2019. Prostaglandin FP receptor antagonists: discovery, pharmacological
829 characterization and therapeutic utility. *Br J Pharmacol* **176**:1059–1078.
830 doi:10.1111/bph.14335

831 Shmuel A, Yacoub E, Pfeuffer J, Moortele P Van De, Adriany G, Hu X, Ugurbil K, Van de
832 Moortele PF, Adriany G, Hu X, Ugurbil K. 2002. Sustained negative BOLD, blood flow and
833 oxygen consumption response and its coupling to the positive response in the human
834 brain. *Neuron* **36**:1195–1210. doi:10.1016/S0896-6273(02)01061-9

835 Smetters D, Majewska A, Yuste R. 1999. Detecting action potentials in neuronal populations
836 with calcium imaging. *Methods: A Companion to Methods in Enzymology* **18**:215–221.
837 doi:10.1006/meth.1999.0774

838 Sun W, McConnell E, Pare J-F, Xu Q, Chen M, Peng W, Lovatt D, Han X, Smith Y, Nedergaard
839 M. 2013. Glutamate-Dependent Neuroglial Calcium Signaling Differs Between Young and
840 Adult Brain. *Science (1979)* **339**:197–200. doi:10.1126/science.1226740

841 Takei S, Hasegawa-Ishii S, Uekawa A, Chiba Y, Umegaki H, Hosokawa M, Woodward DF,
842 Watanabe K, Shimada A. 2012. Immunohistochemical demonstration of increased
843 prostaglandin F2α levels in the rat hippocampus following kainic acid-induced seizures.
844 *Neuroscience* **218**:295–304. doi:10.1016/j.neuroscience.2012.05.013

845 Takemiya T, Matsumura K, Yamagata K. 2007. Roles of prostaglandin synthesis in excitotoxic
846 brain diseases. *Neurochem Int* **51**:112–120. doi:10.1016/j.neuint.2007.05.009

847 Tasic B, Menon V, Nguyen TNTN, Kim TKTTKTK, Jarsky T, Yao Z, Levi BBP, Gray LT, Sorensen SA,
848 Dolbeare T, Bertagnolli D, Goldy J, Shapovalova N, Parry S, Lee CCK, Smith K, Bernard A,
849 Madisen L, Sunkin SM, Hawrylycz M, Koch C, Zeng H, Yao Z, Lee CCK, Shapovalova N, Parry
850 S, Madisen L, Sunkin SM, Hawrylycz M, Koch C, Zeng H. 2016. Adult mouse cortical cell
851 taxonomy revealed by single cell transcriptomics. *Nat Neurosci* **advance on**:1–37.
852 doi:10.1038/nn.4216

853 Team RC, R Core Team, Team RC. 2023. R: A Language and Environment for Statistical
854 Computing.

855 Thévenaz P, Ruttimann UE, Unser M. 1998. A pyramid approach to subpixel registration based
856 on intensity. *IEEE Transactions on Image Processing* **7**:27–41. doi:10.1109/83.650848

857 Tournissac M, Boido D, Omnès M, Goulam-Houssen Y, Ciobanu L, Charpak S. 2022. Cranial
858 window for longitudinal and multimodal imaging of the whole mouse cortex.
859 *Neurophotonics* **9**. doi:10.1117/1.nph.9.3.031921

860 Tran CHT, George AG, Teskey GC, Gordon GR. 2020. Seizures elevate gliovascular unit Ca2+
861 and cause sustained vasoconstriction. *JCI Insight* **5**. doi:10.1172/jci.insight.136469

862 Tsurumaki T, Yamaguchi T, Higuchi H. 2002. Marked neuropeptide Y-induced contractions via
863 NPY-Y1 receptor and its desensitization in rat veins. *Vascul Pharmacol* **39**:325–333.
864 doi:10.1016/S1537-1891(03)00044-2

865 Uhlirova H, Kılıç K, Tian P, Thunemann M, Desjardins M, Saisan PA, Sakadžić S, Ness T V., Mateo
866 C, Cheng Q, Weldy KL, Razoux F, Vandenberghe M, Cremonesi JA, Ferri CGL, Nizar K,
867 Sridhar VB, Steed TC, Abashin M, Fainman Y, Masliah E, Djurovic S, Andreassen OA, Silva
868 GA, Boas DA, Kleinfeld D, Buxton RB, Einevol GT, Dale AM, Devor A, Kılıc K, Tian P,
869 Thunemann M, Ness T V., Saisan PA, Sakadz S, Mateo C, Cheng Q, Weldy KL, Razoux F,
870 Vandenberghe M, Cremonesi JA, Ferri CGL, Nizar K, Sridhar VB, Steed TC, Abashin M, Silva
871 GA, Boas DA, Kleinfeld D, Buxton RB. 2016. Cell type specificity of neurovascular coupling
872 in cerebral cortex. *Elife* **5**:1–23. doi:10.7554/eLife.14315

873 Wagner L, Wolf R, Zeitschel U, Rossner S, Petersén Å, Leavitt BR, Kästner F, Rothermundt M,
874 Gärtner UT, Gündel D, Schlenzig D, Frerker N, Schade J, Manhart S, Rahfeld JU, Demuth
875 HU, Von Hörsten S. 2015. Proteolytic degradation of neuropeptide y (NPY) from head to

876 toe: Identification of novel NPY-cleaving peptidases and potential drug interactions in
877 CNS and Periphery. *J Neurochem* **135**:1019–1037. doi:10.1111/jnc.13378

878 Yamagata K, Andreasson KI, Kaufmann WE, Barnes CA, Worley PF. 1993. Expression of a
879 Mitogen-Inducible Cyclooxygenase in Brain Neurons : Regulation by Synaptic Activity and
880 Glucocorticoids. *Neuron* **11**:371–386. doi:10.1016/0896-6273(93)90192-t

881 Yamagata K, Matsumura K, Inoue W, Shiraki T, Suzuki K, Yasuda S, Sugiura H, Cao C, Watanabe
882 Y, Kobayashi S. 2001. Coexpression of microsomal-type prostaglandin E synthase with
883 cyclooxygenase-2 in brain endothelial cells of rats during endotoxin-induced fever.
884 *Journal of Neuroscience* **21**:2669–2677. doi:10.1523/jneurosci.21-08-02669.2001

885 Zeisel A, Muñoz-Manchado AB, Codeluppi S, Lönnerberg P, La Manno G, Juréus A, Marques S,
886 Munguba H, He L, Betsholtz C, Rolny C, Castelo-Branco G, Hjerling-Leffler J, Linnarsson S.
887 2015. Cell types in the mouse cortex and hippocampus revealed by single-cell RNA-seq.
888 *Science (1979)* **347**:1138–1142.

889 Zhang D, Ruan J, Peng S, Li J, Hu X, Zhang Y, Zhang T, Ge Y, Zhu Z, Xiao X, Zhu YY, Li XX, Li T,
890 Zhou L, Gao Q, Zheng G, Zhao B, Li XX, Zhu YY, Wu J, Li W, Zhao J, Ge W, Xu T, Jia J-M.
891 2024. Synaptic-like transmission between neural axons and arteriolar smooth muscle
892 cells drives cerebral neurovascular coupling. *Nat Neurosci* 1–17. doi:10.1038/s41593-
893 023-01515-0

894 Zhang DY, Raichle ME. 2010. Disease and the brain's dark energy. *Nat Rev Neurol* **6**:15–28.
895 doi:10.1038/nrneurol.2009.198

896 Zhou N, Gordon GRJ, Feighan D, MacVicar BA. 2010. Transient swelling, acidification, and
897 mitochondrial depolarization occurs in neurons but not astrocytes during spreading
898 depression. *Cerebral Cortex* **20**:2614–2624. doi:10.1093/cercor/bhq018

899 Zonta M, Angulo MC, Gobbo S, Rosengarten B, Hossmann K-A, Pozzan T, Carmignoto G. 2003.
900 Neuron-to-astrocyte signaling is central to the dynamic control of brain microcirculation.
901 *Nat Neurosci* **6**:43–50. doi:10.1038/nn980